JOURNAL OF PETROLOGY | VOLUME 42 | NUMBER 1 | PAGES 69–87 | 2001

Metasomatism and Melting in Carbonated Peridotite Xenoliths from the Mantle Wedge: The Gobernador Gregores Case (Southern Patagonia)

ANGELA LAURORA[1], MAURIZIO MAZZUCCHELLI[1]*, GIORGIO RIVALENTI[1], RICCARDO VANNUCCI[2], ALBERTO ZANETTI[2], MARIA ADELAIDE BARBIERI[1] AND CARLOS A. CINGOLANI[3]

[1]DIPARTIMENTO DI SCIENZE DELLA TERRA, UNIVERSITÀ DI MODENA E REGGIO EMILIA, P.LE S. EUFEMIA, 19, I-41100 MODENA, ITALY

[2]DIPARTIMENTO DI SCIENZE DELLA TERRA, UNIVERSITÀ DI PAVIA AND CNR CENTRO DI STUDIO PER LA CRISTALLOCHIMICA E CRISTALLOGRAFIA, VIA FERRATA, 1, I-27100 PAVIA, ITALY

[3]CENTRO DE INVESTIGACIONES GEOLÓGICAS, UNIVERSIDAD NACIONAL DE LA PLATA, 644 CALLE NO. 1, 1900 LA PLATA, ARGENTINA

RECEIVED DECEMBER 16, 1999; REVISED TYPESCRIPT ACCEPTED JUNE 28, 2000

Spinel-facies mantle xenoliths occur in a diatreme cutting through the Neogene Southern Patagonia Plateau at Gobernador Gregores (Santa Cruz Province, Argentina). This plateau is in a back-arc position with respect to the Chile trench. Xenoliths differ in their whole-rock composition from other South America occurrences, having higher CaO/Al_2O_3 ratios and, in some samples, TiO_2 enrichment, whereas the Na_2O/Al_2O_3 variation range is similar. Three assemblages can be distinguished. Assemblage 1, in anhydrous protogranular lherzolites and harzburgites, contains clinopyroxene with a depleted major and trace element composition, indicating pre-metasomatic depletion processes. This assemblage fully recrystallized to Assemblage 2 (amphibole ± phlogopite ± Cl-apatite-bearing) during a metasomatic episode. This causes clinopyroxene to acquire geochemical characteristics often attributed to carbonate-melt metasomatism. Noticeably, amphibole is markedly enriched in Nb (up to 298 ppm), especially when depleted in Ti. A further event, related to decompression during xenolith uplift to the surface, induces closed-system (perhaps with the exception of CO_2 addition) disequilibrium melting of Assemblage 2, dominantly of amphibole. It is found in pockets (where amphibole is a residual phase) consisting of Na–Si-rich glass and carbonate (Mg-rich calcite) drops, and in veins originating from the pockets (Assemblage 3). Euhedral olivine, clinopyroxene and spinel crystallize only in the silicate glass. So do new, euhedral apatite crystals when glass is in contact with previous Assemblage 2 apatite. Textural evidence and comparison with experimental work suggest that silicate glass and carbonates are the result of unmixing of a former homogeneous melt. Because of the different flow rates of carbonate and silicate melt, the xenoliths become enriched in carbonate, which is found in the veins, during their migration. Thus, the high CaO/Al_2O_3 ratio of whole rocks provides inconclusive evidence of carbonatite metasomatism. This factor, and other minor deviations from the expected results of carbonatite metasomatism, lead us to hypothesize an aqueous, Cl-rich fluid, possibly slab derived, as an alternative agent. Amphibole, resulting from reactive porous flow of this agent in the mantle, could fully explain the observed geochemical features, as indicated by estimates of its partition coefficients.

KEY WORDS: *carbonated xenoliths; Gobernador Gregores; LAM–ICP-MS; mantle metasomatism; silicate glass*

*Corresponding author. Telephone: +39-059-417231. Fax: +39-059-417399. E-mail: mazzuc@unimo.it

INTRODUCTION

This paper illustrates a new occurrence of carbonated mantle xenoliths in Southern Patagonia (Gobernador Gregores, Santa Cruz Province). Xenoliths occur in a Plio-Pleistocene cinder cone inside one of the largest diatremes cutting through the Neogene Southern Patagonia Plateau [figs 1, 2 and 3C of Gorring *et al.* (1997)]. These lavas occupy a back-arc position with respect to the Chile trench, ~400 km away to the east (Stern *et al.*, 1990; Gorring *et al.*, 1997, and references therein). The occurrence of mantle xenoliths in association with subduction regions is rare (Vidal *et al.*, 1989; Maury *et al.*, 1992; Szabo *et al.*, 1996) and, as far as we know, carbonated mantle xenoliths are very rare in this context (Szabo *et al.*, 1995). Occurrences of xenoliths containing primary (i.e. not supergenic) carbonate, however, are relatively common in other geological situations (e.g. O'Reilly & Griffin, 1988; Ionov *et al.*, 1993, 1996; Johnson *et al.*, 1996; Ionov, 1998; Norman, 1998) and they may provide first-class evidence of the interaction processes between carbonate-rich melts and peridotite, related geochemical signatures, and the origin of the carbonate component.

Generation of carbonatite melts in mantle at pressure $\geq$2 GPa and their importance as efficient metasomatic agents acting on the mantle lithosphere has been demonstrated by Green & Wallace (1988) and supported by further experimental work (Lee & Wyllie, 1998*a*). Carbonatite-related metasomatism results in peculiar geochemical [high light rare earth element (LREE), La and Ce, and low Hf, Zr and Ti, concentration] and modal (orthopyroxene dissolution and a trend toward wehrlite, presence of apatite) signatures common in xenolith occurrences in both continental and oceanic settings (Yaxley *et al.*, 1991, 1998; Dautria *et al.*, 1992; Hauri *et al.*, 1993; Ionov *et al*, 1993; Rudnick *et al.*, 1993). On the other hand, it has also been demonstrated that the relationship between LREE enrichment–HFSE (high field strength element) depletion and carbonate metasomatic agents is not so straightforward and that other agents or metasomatic processes may lead to results similar to those expected from carbonatite (Zinngrebe & Foley, 1995; Bedini *et al.*, 1997; Vannucci *et al.*, 1998; Zanetti *et al.*, 1999). In subduction zones, Sweeney *et al.* (1992) suggested that metasomatism related to a carbonated component may be common, whereas Rudnick *et al.* (1993) concluded that it is unlikely.

The questions we try to answer in this study are: (1) Is a carbonated component responsible for the metasomatic effects observed in the Gobernador Gregores xenoliths? (2) Is the metasomatic agent related to the subducted slab?

We define carbonate melt as melt with a carbonatite-like composition and carbonated silicate melt as silicate melt containing a carbonate component. Elements are normalized with respect to primitive mantle (Hofmann, 1988).

PETROGRAPHY

All the xenoliths are spinel-facies peridotites. They are rounded and reach a maximum size of 60 cm. The dominant rock type, as found from the examination of 120 samples, is lherzolite (88%), followed by harzburgite (8%), wehrlite (3%) and dunite (1%). Amphibole ($\pm$ phlogopite) occurs in 43% of the xenolith collection. Carbonate, apatite and glass are closely associated in pockets.

Three assemblages, related to successive events and/or representing different depth levels in the sampled mantle segment, can be distinguished. The first (Assemblage 1) occurs in lherzolites and subordinate harzburgites with protogranular texture. These rocks do not contain hydrous phases. All the mineral phases are strained [e.g. kink-bands in olivine (Ol_1) and pyroxenes] and pyroxenes (Cpx_1 and Opx_1) are unmixed and cloudy. Spinel (Spl_1) is interstitial and irregularly shaped, but sometimes it is sub-euhedral. The majority of xenoliths are characterized by a coarse-granular texture (Assemblage 2). Clino- and orthopyroxene (Cpx_2 and Opx_2) do not have appreciable exsolution lamellae and the first exhibits a spongy rim of variable thickness. Olivine recrystallization results in large (up to 5 mm) unstrained crystals (Ol_2). Spinel (Spl_2) often contains sub-euhedral silicate inclusions and occurs as an intergranular embayed phase sometimes showing reaction rims. Amphibole may be abundant; phlogopite is rarer. Only rarely do Assemblages 1 and 2 occur in the same xenolith and, when they do, Assemblage 2 appears as a thin recrystallized rim on Assemblage 1 phases.

A further event (Assemblage 3) affects only Assemblage 2 xenoliths and is documented by the occurrence of silicate glass, containing carbonate droplets, in pockets around amphibole and, subordinately, around the other phases of Assemblage 2 (Fig. 1a, b and d). Glass + carbonate veins originate from the pockets and infiltrate along grain boundaries (Fig. 1c), and more rarely in fractures of matrix olivine. Carbonate drops are separated from the silicate glass by smooth, outwardly convex menisci, in both veins and pockets (Fig. 1c and d). Carbonates are never in contact with the matrix phases, a thin film of silicate glass occurring between them (Fig. 1c and d). New and small (<100 μm) euhedral crystals of olivine (Ol_3), clinopyroxene (Cpx_3), spinel (Spl_3) and rarely Fe–Ti oxides (up to 10 μm) are found only in the silicate glass (Fig. 1a and d).

Large apatite crystals, up to 2 mm across (Fig. 1d), occur in a few samples as cloudy relics rich in partly

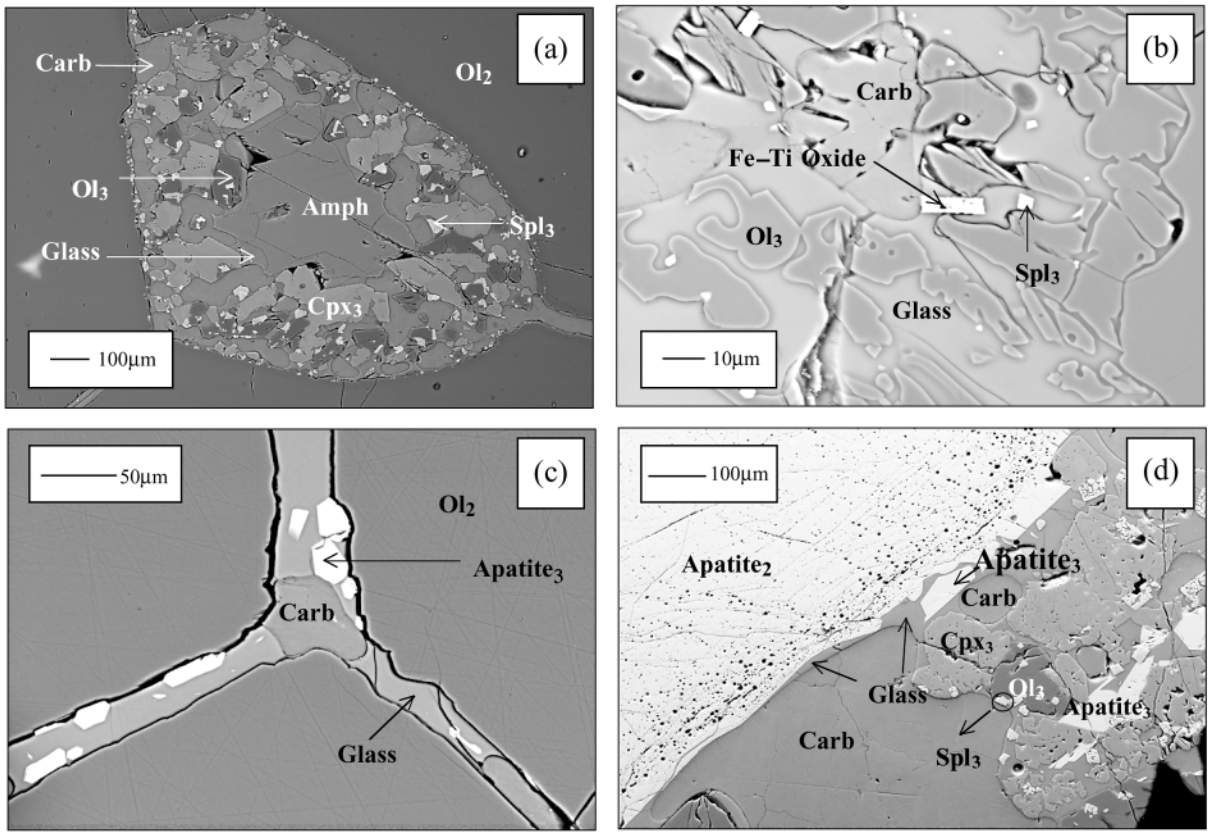

Fig. 1. Back-scattered SEM images of Assemblages 2 and 3. (a) Amphibole (Amph) is the residual phase and three veins originate from the pocket. (b) Assemblage 3 in sample GG92, containing Fe–Ti oxides. (c) Veins in sample GG104 at triple junction between Ol_2 crystals. [Compare this image with fig. 4 of Minarik (1998).] (d) $Apatite_2$ and $Apatite_3$ in sample GG104.

exploded fluid inclusions (<10 μm). Such relics are found immersed in large carbonate pools, but also in contact with the minerals of Assemblage 2 and with glass. Further apatite occurs as inclusion-free euhedral crystals (<10 μm in diameter) in the silicate glass close to, and as a recrystallized rim of, cloudy apatite when this latter is in contact with glass (Fig. 1c and d). Because of its relationship with Assemblage 2, we hereafter refer to cloudy apatite as $Apatite_2$ (even if apatite does not occur in Assemblage 1), whereas the clean euhedral apatite neocrystals are referred to as $Apatite_3$.

As well as in $Apatite_2$, small fluid inclusions occur in all the Assemblage 2 minerals. Preliminary observations indicate that they are predominantly aqueous, CO_2 inclusions being rare even in $Apatite_2$. This contrasts with apatite from other xenolith occurrences, which have compositional and textural characteristics similar to $Apatite_2$, but are commonly rich in CO_2 inclusions (O'Reilly & Griffin, 1988; Yaxley *et al.*, 1991; Chazot *et al.*, 1996).

ANALYTICAL METHODS

Major elements were determined in whole rock by wavelength-dispersive X-ray fluorescence and in mineral phases and glass by electron microprobe at the Earth Sciences Department of Modena University. Details of the analytical technique have been reported by Mazzucchelli *et al.* (1992). Trace element data were obtained by laser ablation microprobe–inductively coupled plasma-mass spectrometry (LAM–ICP-MS) at CSCC, Pavia. The basic setup of the instrument and the analytical protocol have been described by Bottazzi *et al.* (1999), with a major modification to the laser probe consisting in the adoption of a shorter laser wavelength (213 nm) obtained by mixing the fundamental (1064 nm) and the fourth harmonic (266 nm) radiations in a third harmonic generator, in a similar way to that shown by Jeffries *et al.* (1998). At this shorter wavelength, even the carbonates analysed for this study displayed a regular ablation, whereas a first attempt using the 266 nm resulted in the so-called 'catastrophic ablation' that hampered any accurate quantitative determination. NIST SRN 612 was used as the external standard, and ^{44}Ca as the internal standard. Precision and accuracy of trace element analysis were assessed on a control sample BCR2-g (reference values are from USGS Geochemical Reference Materials database, http://minerals.cr.usgs.gov/geo_chem_stand/;

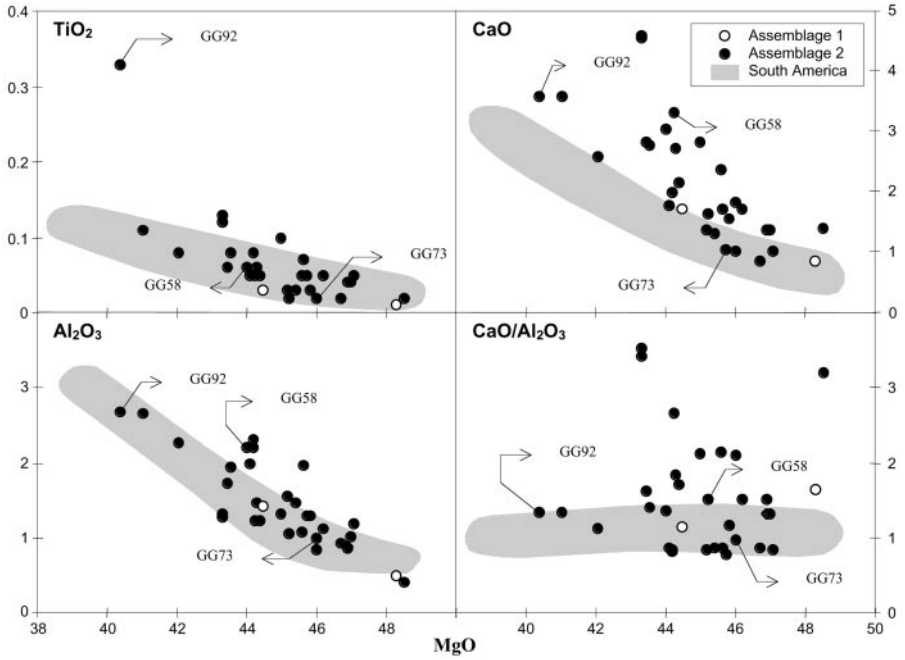

Fig. 2. Selected whole-rock chemical parameters compared with those of other South American xenolith occurrences (data source: Barbieri *et al.*, 1999; Rivalenti *et al.*, 2000). Labelled points refer to the selected samples described in the text.

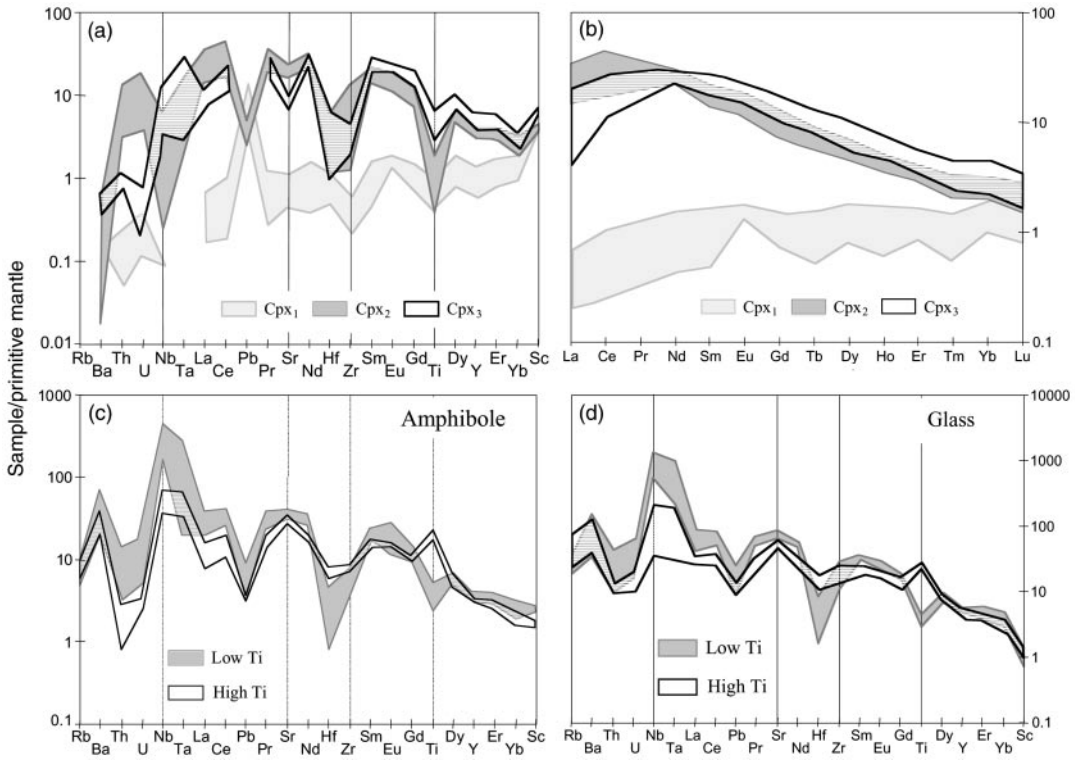

Fig. 3. (a) Trace element patterns of clinopyroxenes of Assemblages 1, 2 and 3. (b) REE patterns of clinopyroxenes. (c) Trace element patterns of high-Ti and low-Ti amphiboles. (d) Trace element patterns of the Assemblage 3 glasses, which mirror the amphibole patterns. In all the diagrams, the sample fields represent 1σ standard deviation from the average. Concentrations are normalized to the Primitive Mantle composition (Hofmann, 1988).

Table 1: Variation range (average ± standard deviation) of some indicative parameters in clinopyroxenes and amphiboles

Phase:	Cpx_1		Cpx_2		Cpx_3		High-Ti Amph		Low-Ti Amph	
No. of samples:	(3)	(1σ)	(11)	(1σ)	(7)	(1σ)	(6)	(1σ)	(2)	(1σ)
TiO_2	0·12	0·06	0·19	0·13	0·53	0·39	3·33	0·28	0·67	0·56
Al_2O_3	2·74	0·39	5·53	0·83	6·28	1·10	13·88	0·07	14·19	0·56
CaO	23·40	0·18	18·77	0·82	21·30	1·03	9·19	0·14	10·21	0·45
Na_2O	0·37	0·11	2·18	0·28	0·73	0·24	3·44	0·14	3·69	0·25
Cr_2O_3	0·76	0·15	1·73	0·27	2·44	0·77	1·12	0·36	2·18	0·33
mg-number	0·93	0·003	0·90[1]	0·005[1]	0·92[1]	0·002[1]	0·85	0·02	0·90	0·004
La_N/Yb_N	0·29	0·15	9·39	2·82	2·88	0·66	6·19	2·22	11·15	3·55
La_N/Nd_N	0·46	0·07	0·90	0·27	0·39	0·05	0·59	0·14	0·90	0·32
Nd_N/Yb_N	0·65	0·32	11·00	3·10	7·52	1·74	10·12	1·43	12·52	2·48
Zr_N/Hf_N	0·57	0·16	3·98	2·83	5·28	4·29	1·10	0·05	4·96	3·98
Sr*	1·00	0·24	0·76	0·06	0·37	0·11	1·79	0·13	1·18	0·08
Zr*	0·42	0·05	0·35	0·26	0·19	0·08	0·46	0·01	0·26	0·10
Ti*	0·75	0·28	0·15	0·26	0·23	0·14	2·34	0·01	0·43	0·15

Oxides in wt %; *mg*-number = molar $MgO/(MgO + FeO_{tot})$; $Sr^* = Sr_N \times 2/(Pr_N + Nd_N)$; $Zr^* = Zr_N \times 2/(Nd_N + Sm_N)$; $Ti^* = Ti_N \times 2/(Gd_N + Dy_N)$.
[1]Sample GG92 (*mg*-number = 0·88 and 0·87 in Cpx_2 and Cpx_3 respectively) is not included.

reference values for Nb, Ta, Dy and Er are ICP-MS unpublished data by Memorial University of Newfoundland, St John's, Canada) to be approximately <7 and 10%, respectively. Detection limits of LAM–ICP-MS analysis are largely a function of ablation volume and the counting time per element. Ablation volume varies strongly depending on the instrumental configuration, and therefore detection limits are calculated for each analysis. As a whole, detection limits degrade if spot size, beam power and cell gas flow are decreased. Trace element analysis of Assemblage 3 minerals was performed using smaller spot size and lower beam power, and therefore higher detection limit values have been obtained for those analyses. In Table 2a and b (see below) element concentrations below detection limit are reported as lower than two times the detection limit value calculated for the analysis.

ANALYTICAL RESULTS

Whole rock

Figure 2 compares the whole-rock composition of the Gobernador Gregores xenoliths (analyses are available on line at the *Journal of Petrology* Web site http://www.petrology.oupjournals.org) with other spinel-facies xenoliths of South America. Assemblage 1 is represented by only three samples. Scanning electron microscopy (SEM) images reveal that carbonate veins thinner than 3 μm occur in all the samples, including those characterized by Assemblage 1 and those that contain only Assemblage 2. Consequently, in Fig. 2 some of the xenoliths show deviations towards higher CaO and CaO/Al_2O_3 values with respect to the other South American xenoliths and with respect to $CaO/Al_2O_3 = 0{\cdot}95$, which is the average value for the sub-continental spinel lherzolite mantle (McDonough, 1990). The Na_2O/Al_2O_3 ratios, <0·04, are comparable with those of the other South American occurrences and much lower than the 0·21–0·55 range of the Yaxley *et al.* (1991) samples and the 0·07–0·48 range of the Rudnick *et al.* (1993) samples. Some samples are also enriched in TiO_2 (e.g. GG92) and in Al_2O_3 (e.g. GG58) with respect to the variation field of the xenoliths reported for comparison.

Mineral phases

Olivine

From Ol_1 to Ol_3, CaO concentration increases (maximum CaO concentration is 0·08, 0·21 and 0·79 wt % in Ol_1, Ol_2 and Ol_3, respectively) and NiO decreases, whereas the more magnesian compositions are found in Ol_3 (Fo from 89·1 to 93·5).

Table 2a: Major (wt %) and trace (ppm) element analyses of Assemblage 2 minerals in the four selected samples

Sample:	GG58								GG73									
Rock type:	wehrlite								lherzolite									
Phase:	Amph		Cpx_2		Ol_2		Spl_2		Amph		Cpx_2		Opx_2		Ol_2		Spl_2	
No. of analyses:	**(3)**	(1σ)	(6)	(1σ)	(3)	(1σ)	(2)	(1σ)	**(3)**	(1σ)	(3)	(1σ)	(3)	(1σ)	(6)	(1σ)	(6)	(1σ)
SiO_2	**42·16**	0·16	53·09	0·05	40·72	0·33	0·09	0·004	**44·89**	0·16	53·19	0·80	56·22	0·20	40·94	0·23	0·05	0·05
TiO_2	**0·61**	0·01	0·10	0·01	0·01	0·01	0·07	0·004	**0·32**	0·02	0·06	0·00	0·02	0·01	0·01	0·01	0·06	0·01
Al_2O_3	**15·07**	0·20	6·69	0·06	0·00	0·00	55·09	0·033	**13·61**	0·06	4·69	0·10	2·42	0·05	0·04	0·02	28·70	0·06
FeO_{tot}	**3·67**	0·06	2·69	0·06	9·53	0·17	10·10	0·076	**3·72**	0·09	2·90	0·15	5·95	0·12	9·17	0·07	16·07	0·11
MnO	**0·06**	0·02	0·09	0·03	0·15	0·01	0·11	0·02	**0·06**	0·04	0·09	0·01	0·18	0·01	0·13	0·02	0·22	0·04
MgO	**18·31**	0·26	14·86	0·52	49·29	0·32	21·62	0·02	**18·61**	0·04	15·72	0·42	33·71	0·06	49·27	0·37	15·34	0·12
CaO	**10·38**	0·12	18·52	0·94	0·06	0·01	0·01	0·004	**11·05**	0·24	19·37	0·73	0·65	0·04	0·05	0·01	0·01	0·02
Na_2O	**4·10**	0·02	2·50	0·04	0·01	0·01	0·00	0·001	**3·60**	0·13	1·76	0·56	0·14	0·01	0·01	0·01	0·01	0·01
K_2O	**1·02**	0·03			0·01	0·00	0·01	0·004	**1·28**	0·02					0·01	0·00	0·01	0·02
P_2O_5																		
Cr_2O_3	**1·75**	0·03	1·34	0·06	0·03	0·02	12·79	0·024	**2·78**	0·02	2·19	0·05	0·65	0·03	0·04	0·02	39·78	0·09
NiO					0·39	0·01	0·34	0·02							0·37	0·04	0·19	0·04
F																		
Cl									**0·07**	0·00								
No. of analyses:	**(3)**	(1σ)	(3)	(1σ)					**(2)**	(1σ)	(2)	(1σ)						
Rb	**5·33**	0·14	<1·1						**4·86**	0·32	<0·4							
Ba	**421**	23	<1·5						**204**	4	<0·5							
Th	**1·35**	0·20	1·28	0·05					**0·57**	0·00	0·48	0·01						
U	**0·33**	0·02	0·39	0·02					**0·25**	0·02	0·24	0·03						
Nb	**73·2**	2·8	0·78	0·07					**250**	10	1·83	0·08						
Ta	**1·35**	0·03	0·10	0·00					**4·85**	0·06	0·11	0·03						
La	**22·9**	1·3	18·8	0·9					**17·8**	0·7	13·0	0·1						
Ce	**61·7**	2·5	54·0	2·0					**58·2**	3·0	44·4	1·2						
Pb	**1·50**	0·12	0·89	0·02					**1·36**	0·16	0·63	0·04						
Pr	**7·60**	0·42	6·83	0·26					**8·23**	0·28	6·49	0·31						
Sr	**649**	10	383	4					**667**	99	384	7						
Nd	**33·9**	1·3	30·7	0·5					**37·4**	0·9	30·2	1·6						
Hf	**0·49**	0·02	0·67	0·06					**0·21**	0·11	0·10	0·03						
Zr	**53·0**	3·4	49·4	1·3					**44·0**	1·8	30·2	1·0						
Sm	**7·37**	0·31	6·74	0·16					**7·76**	0·39	7·67	0·46						
Eu	**2·39**	0·20	2·39	0·05					**2·60**	0·02	2·20	0·04						
Gd	**5·56**	0·32	5·09	0·12					**5·41**	0·18	4·79	0·24						
Dy	**3·85**	0·17	3·99	0·15					**3·51**	0·01	3·36	0·16						
Y	**16·6**	0·6	16·7	0·4					**14·5**	0·4	13·1	0·0						
Er	**1·66**	0·17	1·69	0·12					**1·42**	0·04	1·26	0·11						
Yb	**1·41**	0·13	1·51	0·07					**0·98**	0·05	0·92	0·02						
Sc	**35·8**	0·7	55·4	0·5					**45·8**	2·4	63·2	1·5						

Analyses in bold are used in the mass-balance calculations.

Sample:	GG92											GG104											
Rock type:	lherzolite											lherzolite											
Phase:	Phlog	Amph		Cpx_2		Opx_2		Ol_2		Spl_2		Amph		Cpx_2		Opx_2		Ol_2		Spl_2		Ap_2	
No. of analyses:	(1)	(10)	(1σ)	(2)	(1σ)	(11)	(1σ)	(5)	(1σ)	(2)	(1σ)	(8)	(1σ)	(3)	(1σ)	(3)	(1σ)	(9)	(1σ)	(5)	(1σ)	(14)	(1σ)
SiO_2	**37·27**	**41·46**	0·68	**52·30**	0·05	**54·46**	0·82	40·42	0·14	0·08	0·02	**43·60**	1·02	53·90	0·11	56·00	0·05	41·09	0·56	0·06	0·04		
TiO_2	**3·93**	**3·28**	0·72	**0·23**	0·02	**0·19**	0·09	0·01	0·01	0·46	0·02	**0·38**	0·02	0·04	0·01	0·01	0·01	0·01	0·01	0·10	0·04		
Al_2O_3	**16·30**	**13·81**	0·43	**6·14**	0·01	**4·01**	0·73	0·00	0·00	43·78	0·00	**13·71**	0·30	4·45	0·05	2·61	0·02	0·01	0·01	33·20	2·99		
FeO_{tot}	**5·07**	**5·38**	0·41	**3·72**	0·02	**8·16**	0·72	11·41	0·27	17·76	0·00	**3·62**	0·05	2·77	0·00	6·58	0·08	9·25	0·10	14·67	1·73		
MnO	**0·01**	**0·06**	0·02	**0·10**	0·01	**0·14**	0·02	0·14	0·03	0·18	0·02	**0·06**	0·03	0·11	0·01	0·17	0·03	0·14	0·02	0·21	0·01		
MgO	**20·18**	**15·56**	0·71	**14·65**	0·07	**31·50**	0·56	47·26	0·74	17·19	0·15	**18·58**	0·78	15·59	0·16	33·23	0·06	49·64	1·91	17·10	1·36	1·48	0·17
CaO	**0·01**	**9·33**	0·40	**18·50**	0·09	**0·88**	0·16	0·06	0·03	0·02	0·00	**10·99**	0·36	19·27	0·23	0·65	0·00	0·07	0·01	0·02	0·03	51·97	0·77
Na_2O	**0·96**	**3·31**	0·04	**2·52**	0·01	**0·22**	0·10	0·02	0·01	0·00	0·00	**3·48**	0·11	2·04	0·01	0·13	0·00	0·01	0·01	0·07	0·10	0·91	0·12
K_2O	**9·29**	**1·62**	0·07					0·00	0·00	0·01	0·01	**1·50**	0·04					0·00	0·00	0·02	0·04		
P_2O_5																						40·48	0·83
Cr_2O_3	**0·19**	**0·76**	0·51	**1·56**	0·01	**0·29**	0·16	0·01	0·01	20·61	0·14	**2·46**	0·05	1·78	0·03	0·57	0·03	0·02	0·02	34·73	2·77		
NiO	**0·51**							0·42	0·03	0·31	0·00							0·39	0·06	0·24	0·04		
F																						0·55	0·19
Cl	**0·01**	**0·02**	0·01									**0·07**	0·07									2·00	0·07
No. of analyses:	(1)	(2)	(1σ)	(2)	(1σ)							(2)	(1σ)	(1)								(2)	(1σ)
Rb	**263**	**5·90**	0·43	<1								**5·54**	0·09	<0·8								<0·6	
Ba	**4171**	**222**	17	<0·4								**427**	3	<0·5								383	9
Th	<0·01	**0·22**	0·03	**0·27**	0·05							**1·15**	0·06	0·95								218	9
U	**0·01**	**0·07**	0·08	**0·07**	0·00							**0·40**	0·00	0·39								68·2	5·0
Nb	**30·7**	**22·7**	2·7	**0·49**	0·11							**295**	4	1·99								0·86	0·01
Ta	**1·71**	**1·19**	0·12	**0·16**	0·00							**10·1**	0·0	0·24								<0·04	
La	<0·1	**9·17**	0·60	**12·7**	2·2							**22·8**	0·2	16·0								2246	96
Ce	**0·07**	**32·7**	1·1	**47·3**	5·4							**64·9**	0·0	48·7								3217	173
Pb	**0·68**	**0·59**	0·03	**0·88**	0·00							**1·25**	0·04	0·53								13·8	0·8
Pr	<0·04	**4·84**	0·21	**6·69**	0·13							**8·33**	0·05	6·77								291	19
Sr	**303**	**612**	51	**333**	30							**659**	9	386								10690	123
Nd	<0·07	**24·4**	0·5	**30·9**	1·0							**36·5**	2·1	29·0								1078	73
Hf	**0·54**	**2·18**	0·08	**2·27**	0·79							**0·18**	0·02	0·18								<0·07	
Zr	**24·7**	**82·7**	4·9	**89·7**	19·0							**81·4**	2·3	63·2								6·32	0·35
Sm	<0·2	**6·05**	0·70	**6·78**	0·64							**7·34**	0·54	5·80								128	11
Eu	**0·07**	2·20	0·09	**2·44**	0·20							**2·30**	0·06	1·92								31·8	3·4
Gd	<0·5	**5·05**	0·37	**4·13**	0·45							**5·01**	0·05	4·48								81·4	7·8
Dy	<0·2	**2·92**	0·12	**3·78**	0·08							**2·95**	0·14	2·83								37·2	4·0
Y	<0·1	**12·3**	0·0	**13·9**	0·9							**12·4**	0·8	11·7								118	4
Er	<0·1	**1·09**	0·13	**1·63**	0·27							**1·16**	0·07	1·27								9·51	0·91
Yb	<0·06	**0·74**	0·03	**1·11**	0·09							**0·88**	0·20	1·17								5·98	0·51
Sc	**4·52**	**26·2**	2·2	**60·8**	0·3							**37·4**	2·1	54·4								1·05	0·52

Analyses in bold are used in the mass-balance calculations.

Table 2b: Major (wt %) and trace (ppm) element analyses of Assemblage 3 minerals in the four selected samples

Sample:	GG58								GG73								GG92								
Rock:	wehrlite								lherzolite								lherzolite								
Phase:	Cpx_3		Ol_3		Spl_3		Glass		Cpx_3		Ol_3		Spl_3		Glass		Cpx_3		Ol_3		Spl_3	Glass		Carb	
No. of analyses:	(5)	(1σ)	(3)	(1σ)	(4)	(1σ)	(2)	(1σ)	(3)	(1σ)	(3)	(1σ)	(4)	(1σ)	(5)	(1σ)	(3)	(1σ)	(2)	(1σ)	(1)	(10)	(1σ)	(2)	(1σ)
SiO_2	**50·04**	1·16	**40·70**	0·39	**0·10**	0·02	**51·45**	0·11	**48·76**	0·67	**41·30**	0·23	**0·45**	0·23	**50·95**	0·63	**50·06**	0·74	**41·02**	0·03	**0·11**	**50·61**	1·05		
TiO_2	**0·51**	0·13	**0·01**	0·00	**0·20**	0·01	**0·76**	0·01	**0·47**	0·01	**0·01**	0·01	**0·37**	0·06	**0·49**	0·03	**1·66**	0·10	**0·12**	0·07	**0·26**	**3·28**	0·63		
Al_2O_3	**7·19**	1·54	**0·20**	0·23	**50·56**	2·99	**25·23**	0·08	**6·66**	0·11	**0·05**	0·04	**36·74**	4·36	**22·34**	0·45	**5·59**	0·50	**0·27**	0·27	**46·08**	**20·00**	1·33		
FeO_{tot}	**2·26**	0·09	**6·83**	0·28	**9·09**	0·32	**3·18**	0·12	**2·12**	0·00	**6·43**	0·13	**11·10**	0·81	**3·01**	0·24	**4·62**	0·51	**9·93**	0·32	**12·17**	**4·21**	0·53	**0·14**	0·15
MnO	**0·05**	0·03	**0·12**	0·00	**0·11**	0·03	**0·09**	0·01	**0·04**	0·01	**0·11**	0·03	**0·14**	0·04	**0·05**	0·04	**0·10**	0·02	**0·14**	0·01	**0·13**	**0·07**	0·02		
MgO	**14·90**	0·91	**51·93**	1·00	**20·79**	0·40	**4·19**	0·05	**14·45**	0·24	**51·26**	0·20	**19·57**	0·53	**3·83**	0·38	**16·95**	0·51	**47·33**	0·29	**19·54**	**4·06**	0·55	**2·68**	0·21
CaO	**21·62**	1·30	**0·27**	0·07	**0·06**	0·01	**8·73**	0·09	**23·37**	0·64	**0·29**	0·02	**0·19**	0·10	**7·72**	0·66	**19·47**	0·68	**0·30**	0·02	0·06	**9·53**	1·03	**52·84**	0·11
Na_2O	**1·04**	0·26	**0·07**	0·10	**0·05**	0·08	**8·12**	0·17	**0·33**	0·15	**0·01**	0·00	**0·02**	0·02	**7·84**	1·32	**0·51**	0·11	**0·02**	0·01	**0·05**	**3·77**	0·59		
K_2O			**0·03**	0·03	**0·02**	0·03	**1·74**	0·09			**0·01**	0·00	**0·03**	0·02	**1·95**	0·15			**0·01**	0·01	**0·02**	**2·67**	0·54		
P_2O_5																									
Cr_2O_3	**2·26**	0·51	**0·09**	0·02	**18·88**	2·26	**0·03**	0·01	**3·72**	0·31	**0·37**	0·15	**31·36**	4·27	**0·36**	0·30	**0·94**	0·54	**0·09**	0·01	**21·75**	**0·04**	0·02		
NiO			**0·36**	0·02	**0·32**	0·01	**0·01**	0·01			**0·36**	0·04	**0·33**	0·03	**0·05**	0·03			**0·34**	0·05	**0·29**	**0·00**	0·02		
F																									
Cl							**0·11**								**0·16**							**0·04**	0·06		
No. of analyses:	(1)						(2)	(1σ)	(2)	(1σ)					(2)	(1σ)	(2)	(1σ)				(3)	(1σ)	(3)	(1σ)
Rb	<2·4						**12·1**	1·0	**<2·5**						**16·0**	3·0	<2·1					44·5	8·5	<1·3	
Ba	<1·5						**701**	38	<1·8						**495**	29	<1·2					**715**	194	**23·6**	2·5
Th	**0·09**						**3·89**	0·23	**0·03**	0·01					**1·73**	0·31	**0·47**	0·16				**0·84**	0·21	**0·01**	0·00
U	<0·02						**1·03**	0·07	**0·005**	0·001					**0·72**	0·17	**0·11**	0·07				**0·29**	0·09	**1·90**	0·11
Nb	**1·82**						**144**	3	**2·93**	0·59					**432**	17	**0·47**	0·09				**40·1**	4·2	**0·22**	0·03
Ta	<0·1						**2·71**	0·01	**0·23**	0·06					**9·39**	0·63	<0·1					**1·89**	0·21	<0·1	
La	**7·01**						**53·2**	1·3	**4·50**	0·05					**38·3**	4·2	**19·2**	2·7				**19·6**	1·4	<0·5	
Ce	**29·2**						**122**	1	**21·9**	0·8					**110**	6	**58·3**	3·5				**58·8**	3·8	<0·07	
Pb	<1						**5·35**	0·38	<1						**3·41**	0·00	<0·8					**1·46**	0·69	<1·6	
Pr	**5·74**						**14·2**	0·2	**4·50**	0·22					**13·6**	1·1	**7·72**	0·31				**7·15**	0·31	**0·03**	0·00
Sr	**141**						**1382**	12	**111**	2					**1281**	115	**371**	7				**824**	37	**577**	74
Nd	**30·5**						**59·0**	2·1	**26·6**	0·6					**58·6**	5·9	**29·3**	1·4				**33·6**	3·1	<0·2	
Hf	**0·93**						**0·96**	0·05	**0·36**	0·00					<0·6		**0·57**	0·09				**3·52**	0·79	**0·10**	0·05
Zr	**54·5**						**122**	2	**29·1**	3·9					**82·8**	15·0	**43·8**	1·8				**143**	11	**1·30**	0·06
Sm	**9·46**						**11·7**	0·5	**8·96**	0·43					**12·2**	0·5	**4·93**	0·61				**7·37**	0·82	**0·01**	0·00
Eu	**3·33**						**3·17**	0·04	**2·81**	0·16					**3·14**	0·23	**1·53**	0·09				**2·64**	0·26	<0·15	
Gd	**8·77**						**8·50**	0·37	**7·39**	0·35					**7·52**	0·53	**3·44**	0·68				**6·26**	1·01	<1·5	
Dy	**6·45**						**5·59**	0·40	**4·70**	0·26					**4·47**	1·00	**2·57**	0·01				**4·51**	0·26	<0·15	
Y	**25·7**						**25·0**	0·4	**15·3**	0·81					**19·3**	2·3	**11·9**	0·6				**15·1**	1·5	<0·3	
Er	**2·39**						**2·48**	0·03	**1·67**	0·20					**1·66**	0·50	**1·29**	0·21				**1·60**	0·29	**0·06**	0·00
Yb	**2·60**						**2·21**	0·27	**1·19**	0·03					**1·34**	0·36	**1·33**	0·19				**1·06**	0·22	<0·1	
Sc	**112**						**13·7**	0·9	**102**	2					**13·1**	0·0	**61·9**	1·8				**19·6**	1·9	<3	

Table 2b: continued

Sample:	GG104									
Rock:	lherzolite									
Phase:	Cpx_3		Ol_3		Spl_3		Glass		Carb	
No. of analyses:	(6)	(1σ)	(3)	(1σ)	(2)	(1σ)	(4)	(1σ)	(1)	(1σ)
SiO_2	**50·18**	1·30	**40·76**	0·29	**0·16**	0·05	**51·31**	1·94		
TiO_2	**0·46**	0·15	**0·02**	0·03	**0·16**	0·02	**0·52**	0·01		
Al_2O_3	**6·71**	1·36	**0·69**	0·94	**46·77**	2·45	**23·56**	0·59		
FeO_{tot}	**2·25**	0·20	**7·22**	0·26	**10·10**	0·06	**3·32**	0·50	**0·14**	
MnO	**0·04**	0·02	**0·13**	0·01	**0·14**	0·02	**0·07**	0·01		
MgO	**15·28**	1·16	**50·42**	1·33	**20·83**	0·34	**3·30**	0·43	**2·82**	
CaO	**21·51**	1·90	**0·36**	0·30	**0·16**	0·08	**7·44**	0·55	**52·52**	
Na_2O	**0·79**	0·30	**0·02**	0·01	**0·01**	0·01	**6·70**	0·59		
K_2O			**0·03**	0·04	**0·01**	0·01	**3·44**	0·76		
P_2O_5										
Cr_2O_3	**2·74**	0·60	**0·09**	0·01	**21·66**	2·87	**0·39**	0·55		
NiO			0·24	0·02	0·29	0·03	**0·06**	0·03		
F										
Cl							0·26	0·16		
No. of analyses:	(2)	(1σ)					(2)	(1σ)	(6)	(1σ)
Rb	<2						**22·3**	5·3		
Ba	**4·04**	0·00					**1123**	192	**29·1**	7·4
Th	<0·1						**3·73**	0·56	**0·23**	0·27
U	<0·05						**1·41**	0·27	**2·27**	0·35
Nb	**8·57**	0·27					**640**	94	**2·78**	0·39
Ta	**1·14**	0·40					**22·3**	3·5	<0·08	
La	**7·34**	0·65					**62·6**	10·0	**4·19**	2·34
Ce	**34·1**	0·4					**139**	15	**10·9**	11·0
Pb	<0·8						**3·61**	0·22	**1·19**	0·00
Pr	**6·29**	0·37					**16·8**	2·3	**1·01**	0·65
Sr	**178**	1					**1596**	272	**450**	141
Nd	**32·4**	2·5					**60·7**	9·8	**3·55**	2·04
Hf	0·22	0·00					**0·42**	0·09	**0·03**	0·03
Zr	**49·0**	2·0					**156**	23	**1·31**	0·66
Sm	**8·45**	0·18					**12·2**	2·5	**0·87**	0·60
Eu	2·66	0·16					**3·92**	0·26	<0·3	
Gd	6·17	0·01					**7·34**	1·01	<1	
Dy	5·08	0·10					**4·45**	0·54	**0·29**	0·05
Y	**18·4**	0·6					**18·9**	2·2	**0·54**	0·26
Er	**1·92**	0·11					**1·88**	0·32	<0·2	
Yb	**1·36**	0·19					**1·43**	0·23	**0·11**	0·00
Sc	**96·4**	1·5					**9·85**	0·40	<2	

Analyses in bold are used in the mass-balance calculations.

Clinopyroxene

Selected chemical parameters are reported in Table 1. Cpx_1 has the highest *mg*-number and low concentrations of TiO_2, Al_2O_3 and Na_2O (Table 1). Trace element patterns (Fig. 3a and b) display low heavy rare earth element (HREE) concentrations (Yb_N = 0·22–1·99), LREE depletion, almost flat profile from Sm to Yb, negative Zr and Ti anomalies, virtually absent Sr anomaly and Nb below the detection limit. Similar depleted compositions are common in the entire Patagonia mantle lithosphere (Barbieri *et al.*, 1999).

Cpx_2 has lower *mg*-number than Cpx_1 and higher concentrations of TiO_2, Al_2O_3 and Na_2O (Table 1). Cr_2O_3 concentration is as high as 2·21 wt %. The incompatible trace element concentration is dramatically higher than in Cpx_1; REE profiles are LREE enriched and smoothly fractionated from LREE to Yb. Ti and Zr are depleted with respect to REE, Zr_N/Hf_N is >1 and Nb is depleted with respect to La and U (Fig. 3a and b).

Cpx_3 has a very narrow *mg*-number variation range. It is enriched on average, with respect to the other clinopyroxenes, in TiO_2, Al_2O_3, Cr_2O_3 and, with respect to Cpx_2, it has lower Na_2O concentrations (Table 1). One sample (GG92) has lower *mg*-number (0·87) and Cr_2O_3 (0·94 wt %) than the other analysed Cpx_3. Cpx_3

is slightly LREE depleted with respect to Cpx_2 (Table 1) and has higher Nd to Yb concentrations (Fig. 3b). It also differs from Cpx_2 in having a more modest negative Ti anomaly, a negative Sr anomaly (Table 1), enrichment in Nb and Ta (up to 8·84 and 1·17 ppm, respectively) and depletion in U and Th (Fig. 3a).

Orthopyroxene

As observed in clinopyroxene, Opx_2 has slightly lower *mg*-number range than Opx_1 (0·89–0·91 and 0·90–0·91, respectively), and higher Al_2O_3 (2·43–6·86 wt % and 2·64–3·38 wt %, respectively), TiO_2 (0·03–0·37 wt % and 0·02–0·07 wt %, respectively) and Na_2O (0·13–0·25 wt % and 0·00–0·08 wt %, respectively). REE concentrations are at or below the detection limit in Opx_1. The most enriched has $Ce_N = 0·01$ (GG71) and $Yb_N = 0·40$. Opx_2 is distinctly enriched in REE with respect to Opx_1, although concentrations are always low. It often has spoon-shaped patterns with Ce_N ranging from 0·42 to 1·4 and $Yb_N = 0·22–0·77$.

Amphibole

Here it is a pargasite, which may contain up to 0·15 wt % Cl. TiO_2 concentration differentiates the amphiboles into two groups: one with 0·34–1·10 wt % TiO_2 and the other with 3·28–3·90 wt % TiO_2. The first group has higher *mg*-number and Cr_2O_3 concentration than the high-Ti group (Table 1). Both groups have LREE-enriched, smoothly fractionated, REE patterns (Fig. 3c), but the low-Ti amphiboles have slightly higher La_N/Yb_N than the others (Table 1). With respect to the high-Ti amphiboles, the low-Ti ones are enriched in Sr, Nb, Ba, Th and U and have more marked positive Ba and Nb and negative Ti and Hf, spikes (Fig. 3c). High-Ti amphiboles have a positive Ti anomaly. The Zr/Hf ratio is high in the low-Ti amphiboles, whereas these elements are virtually unfractionated in the high-Ti group (Table 1). Similar variability in the amphibole composition was found by Ionov & Hofmann (1995) and Yaxley & Kamenetsky (1999).

Phlogopite

Its composition is variable from one sample to another, *mg*-number and TiO_2 ranging from 0·88 to 0·91 and from 1·8 to 3·9 wt %, respectively. The TiO_2 concentration of phlogopite correlates with that of the coexisting phases. The REE concentrations are close to or below the detection limit. This phase has high concentrations of LILE (Rb = 93–288 ppm, Ba = 2612–4677 ppm) and Nb (30–380 ppm).

Carbonate

It is a Mg-rich calcite with $CaCO_3 \sim 93·5$ wt %, $MgCO_3 \sim 6$ wt % and $FeCO_3 \sim 0·5$ wt %. The *mg*-number and *ca*-number [molar CaO/(CaO + MgO)], ~0·95 and 0·93, respectively, match the values experimentally obtained for carbonates coexisting with spinel-facies peridotites (Dalton & Wood, 1993*a*, 1993*b*).

Apatite

$Apatite_2$ is a Cl-apatite (Cl = 1·8–2·1 wt %, F = 0·34–0·55 wt %). Similar Cl-rich apatites were described by Chazot *et al.* (1996) in Yemen xenoliths and by O'Reilly & Griffin (1988) in Western Victoria, and attributed to metasomatism by carbonatite and $CO_2 + H_2O + Cl$ fluids, respectively. $Apatite_2$ has high LREE concentrations ($La_N = 2877–3814$) and fractionated REE patterns ($La_N/Yb_N = 204–265$), high Sr and Ba concentrations (8270–10813 ppm and 350–412 ppm, respectively) and low Nb and Zr concentrations; Ta and Hf concentration are below the detection limits. The dimensions of $Apatite_3$ do not permit electron microprobe analyses.

Glass

Glass composition does not vary from pockets to veins, but varies from sample to sample and depending on the phase occurring as the reactant inside the pockets. The most common compositions are trachy-basalt and tephriphonolite ($SiO_2 = 48·6–62·6$ wt %), with Al_2O_3 concentrations varying between 13·2 and 24·6 wt %. Most glasses have total alkalis >3·5 wt %, reaching values as high as 11·7 wt %, and $Na_2O/K_2O > 2$. However, when phlogopite is a residual phase, Na_2O/K_2O is <1·5. The glass occurring in sample GG104, associated with large $Apatite_2$ crystals, is one of the lowest in TiO_2 (<0·6 wt %) and one of the highest in Al_2O_3 (>23 wt %) and Na_2O (>6 wt %). Glasses contain up to 0·43 wt % Cl. The trace element pattern of the glasses mirrors that of coexisting amphibole, but with slightly higher element concentrations, markedly higher for Th and U.

Special samples

Four samples, representing examples of the variations in mineral composition and phase relationships previously shown, have been studied in detail. Their whole-rock composition is shown in Fig. 1, except for GG104, which was too small (5 cm in diameter) for whole-rock analyses. Phase composition is reported in Table 2a and b and shown in Fig. 4. Reactant phases (i.e. the phases that are disappearing in the pockets) are amphibole in GG58, GG73 and GG104, whereas GG92 represents a very complex situation, where abundant glass is produced by destabilization of all the Assemblage 2 phases, including phlogopite. Sample GG92 exhibits TiO_2 enrichment in whole-rock and phase compositions, with the latter having

the lowest *mg*-number values (Table 1). GG92 and GG104 contain large $Apatite_2$ and small $Apatite_3$ crystals, and sample GG92 has traces of Fe–Ti oxides in the reaction products. In all the samples, glass composition mirrors that of amphibole (compare the respective patterns in Fig. 4). The carbonate drops in GG58 and GG73 are too small (<20 μm) for major and trace element analyses. However, SEM images reveal that they are Mg-calcites, as in the other samples. The carbonates (GG92 and GG104) resemble those analysed by Ionov (1998). They are slightly LREE enriched, and have REE concentrations close to or below the detection limit and show positive Ba, U and Sr spikes (Fig. 4c and d).

Element distribution between amphibole and Cpx_2 and between Cpx_3 and glass is shown in Fig. 5a and b. The $^{Amph–Cpx2}D_{REE,Y,\,Zr,\,Hf}$ values are parallel to, and from Sr to Yb slightly lower than, the West Eifel data of Witt-Eickschsen & Harte (1994). Most $^{Cpx3–glass}D$ values are within the range observed by Chazot *et al.* (1996).

Equilibration temperature and pressure

The average temperatures calculated at 1·6 GPa (Brey & Köhler, 1990, geothermometer) are 960 ± 98°C and 1090 ± 95°C in Assemblages 1 and 2, respectively. Data on Assemblage 1 refer to exsolved pyroxene pairs. The lack of orthopyroxene in Assemblage 3 does not permit calculation of the two-pyroxene temperature. On the basis of the amphibole stability field, a minimum temperature of ∼1100°C is estimated. Spinel-facies assemblages do not permit estimation of precise pressure conditions. High-precision ICP-MS analyses on the CaO concentration in olivine are not available at present. Using the electron microprobe determinations and the Köhler & Brey (1990) geobarometer, Assemblage 2 ranges from 1·4 to 2·1 GPa. Assemblage 3, assuming a temperature of 1100°C, provides a wide range of pressure estimates from negative values to 1·3 GPa, possibly as a consequence of the difference between Assemblage 3 and the experimental system on which the geobarometer was calibrated.

DISCUSSION

The textural and geochemical characteristics presented so far indicate that at Gobernador Gregores a mantle lithosphere that suffered ancient depletion events subsequently underwent metasomatic enrichment and melting episodes recorded by Assemblages 2 and 3. Hereafter we discuss the petrological indications provided by these two assemblages and show that there is evidence for only one enrichment episode recorded in Assemblage 2. Assemblage 3 is the consequence only of melting and element redistribution of Assemblage 2 and does not require any addition of further metasomatic agents, with the possible exception of low amounts of CO_2.

Assemblage 3: evidence for only one metasomatic episode

We used simple mass-balance calculations applied to special samples to demonstrate that Assemblage 3 resulted from modal melting of Assemblage 2 in a closed system (i.e. isochemical, with the possible exception of CO_2). On the basis of major elements, the results are as follows (in wt %):

$$\text{GG58: 1Amph} = 0{\cdot}29Cpx_3 + 0{\cdot}39\text{Glass} + 0{\cdot}24Ol_3 + 0{\cdot}06Spl_3 + 0{\cdot}02\text{Carb},\ R^2 = 0{\cdot}56;$$

$$\text{GG73: 1Amph} = 0{\cdot}26Cpx_3 + 0{\cdot}43\text{Glass} + 0{\cdot}24Ol_3 + 0{\cdot}05Spl_3 + 0{\cdot}02\text{Carb},\ R^2 = 0{\cdot}26;$$

$$\text{G104: 1Amph} = 0{\cdot}21Cpx_3 + 0{\cdot}46\text{Glass} + 0{\cdot}25Ol_3 + 0{\cdot}05Spl_3 + 0{\cdot}02\text{Carb},\ R^2 = 0{\cdot}93;$$

where R^2 is the sum of the squared residuals. A deduced carbonate composition (that of sample GG104) was used for GG58 and GG73, where direct carbonate analysis was impossible. The carbonate component was introduced in the mass balance as wt % of MgO and CaO. The resulting carbonate component (2 wt %) requires a minimum addition of ∼1·6 wt % CO_2 to the reactant assemblage.

Petrographic examination indicates that in sample GG92 virtually all the phases of Assemblage 2 reacted to produce Assemblage 3. Mass-balance results may, therefore, be of questionable significance. Our best result, which has, however, Spl_3 in the reactants, is as follows:

$$\text{GG92: 1Amph} + 0{\cdot}30Cpx_2 + 0{\cdot}68Opx_2 + 0{\cdot}05Spl_3 + 0{\cdot}15\text{Phlog} = 0{\cdot}18Cpx_3 + 1{\cdot}17\text{Glass} + 0{\cdot}82Ol_3 + 0{\cdot}11\text{Carb},\ R^2 = 0{\cdot}\ 01.$$

In the four cases examined, including GG92, the trace element concentration of the glass calculated using the mass-balance parameters is in close agreement with the measured glass composition (Fig. 4). This provides independent evidence that the geochemical budget of Assemblage 3 is entirely controlled by the modal disequilibrium melting of the metasomatic Assemblage 2 phases, producing a carbonated silicate melt. The composition of this latter was only (GG58, GG73, GG104) or dominantly (GG92) controlled by amphibole. Similar results were reached by Chazot *et al.* (1996) for the origin of glass pockets of xenoliths from Yemen, and Yaxley & Kamenetsky (1999) for glasses from xenoliths from Australia. Calculated glasses for GG92 and GG104 samples have slightly lower U, Th and La concentrations relative to the observed ones (Fig. 4). These differences are explained by the preferential partitioning of these elements into apatite, which was not introduced in

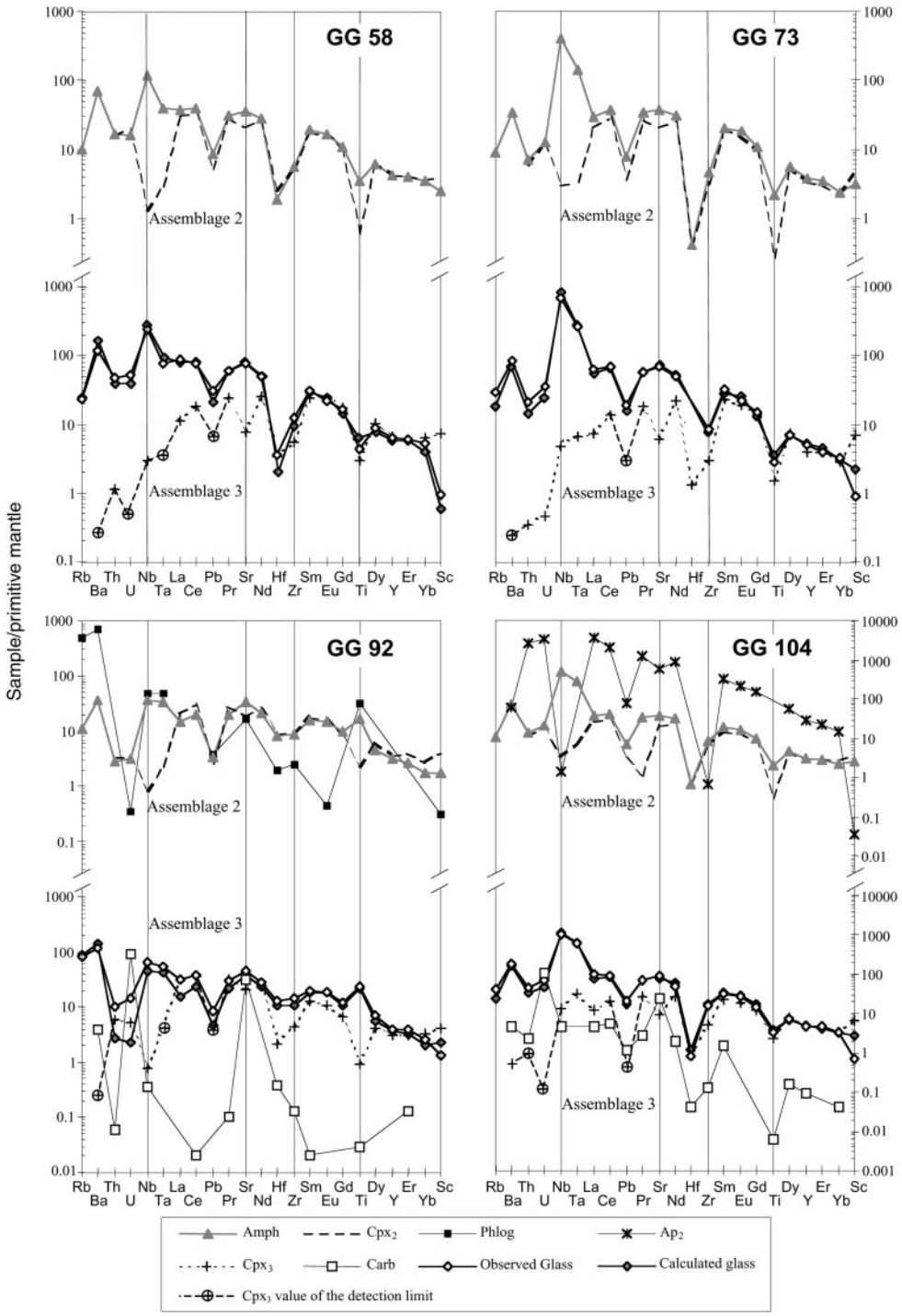

Fig. 4. Trace element characteristics of the Assemblage 2 and Assemblage 3 phases in the four selected samples, normalized to the Primitive Mantle composition (Hofmann, 1988). Values of the detection limit are reported only for Cpx_3. Glass calculated from mass-balance parameters (see text) is compared with the composition of the analysed glass.

the mass-balance calculation because of the difficulty of analysing P in the glass, and the very small dimensions of the $Apatite_3$. The minimal deviation between calculated and observed glass composition even for the elements enriched in apatite, in any case, suggests its limited participation in the melting assemblage, as observed

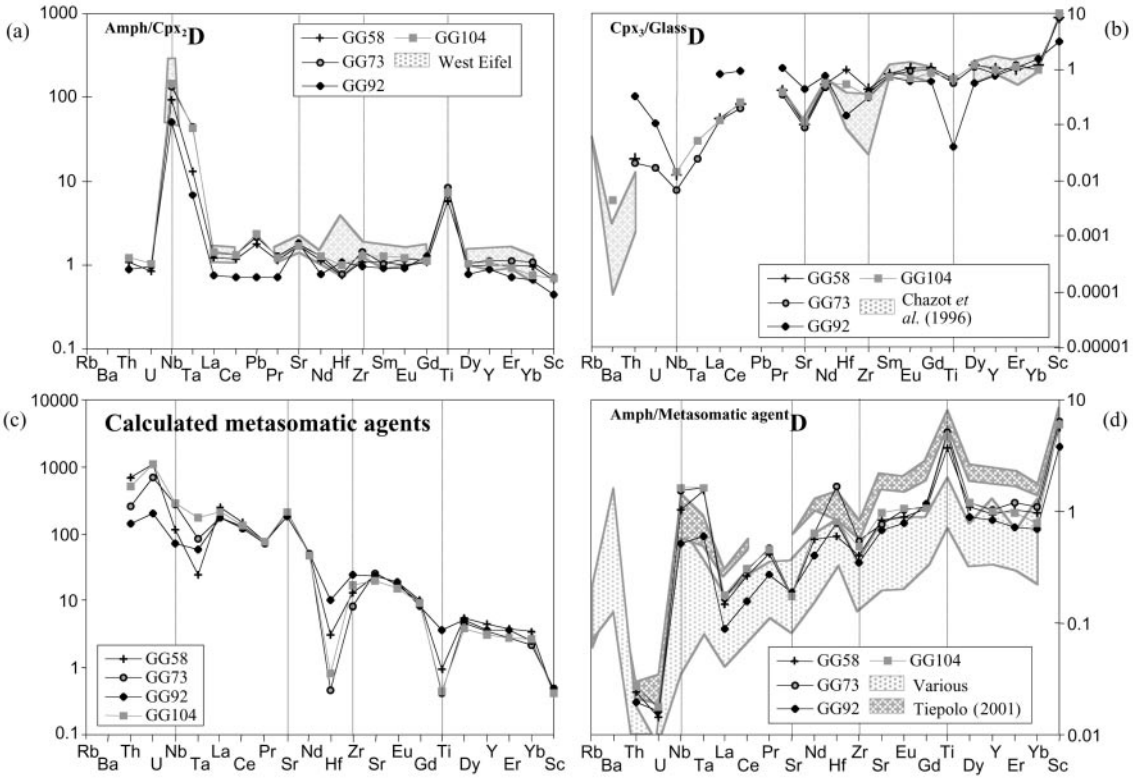

Fig. 5. (a) Amphibole–Cpx_2 partition coefficients compared with the West Eifel data (Witt-Eickschen & Harte, 1994). (b) Cpx_3–glass partition coefficients compared with the data from Chazot *et al.* (1996). (c) Putative metasomatic agent calculated from Cpx_2 composition and $^{Cpx3-Glass}D$ values. (d) Element partitioning between amphibole and the putative metasomatic agent, compared with $^{Amph-Glass}D$ values from McKenzie & O'Nions (1991), Adam *et al.* (1993), Adam & Green (1994), Dalpé & Baker (1994), Brenan *et al.* (1995) and Chazot *et al.* (1996) (light-shaded). The dark shaded area refers to $^{Amph-Glass}D$ values from Tiepolo (1999) and Tiepolo *et al.* (2000, 2001).

elsewhere by O'Reilly & Griffin (1988) and Chazot *et al.* (1996). Further support for negligible $Apatite_2$ participation in melt production is provided by Cl: in sample GG104, which has large $Apatite_2$ crystals, Cl concentration is 0·07, 2 and 0·26 wt % in amphibole, apatite and glass, respectively. Using the mass-balance parameters, the Cl concentration in the calculated glass is 0·18 wt %, requiring, therefore, melting of only 4% apatite to reach the 0·26 wt % Cl concentration observed in the glass. Water was not considered in the mass-balance calculations. Mass balance also does not explain the origin of CO_2 present in the carbonated silicate melt. The complete lack of carbonates in Assemblage 2 either as a separate phase or as inclusions in the silicates, and the dominant aqueous composition of fluid inclusions in the mineral phases suggest either that the system was open to CO_2 during melting or that hypothetical Assemblage 2 carbonates were completely exhausted in the reaction. Open-system CO_2 addition may result from degassing of the host basalts (which contain abundant vesicles filled with carbonates) possibly related to a decrease in pressure during their emplacement (O'Reilly & Griffin, 1988; O'Reilly *et al.*, 1991; Ionov *et al.*, 1994; Ionov, 1998). Specific research on the origin of the CO_2, as well as a detailed study on the fluid inclusions, is under way.

Notwithstanding the CO_2 problem, mass-balance calculations, and the independent evidence provided by trace elements, indicate that the formation of Assemblage 3 post-dates the metasomatism that created Assemblage 2. It is also clear that the Assemblage 3 carbonated melt does not represent a metasomatic agent, but only a breakdown product that was formed during decompression and high-temperature transport in the host magma.

Silicate glass–carbonate relationships: liquid immiscibility vs fractional crystallization

The silicate glass–carbonate relationships observed in the Assemblage 3 pockets and in the veins could be explained by either liquid immiscibility (Pyle & Haggerty, 1994; Kogarko *et al.*, 1995) or fractional crystallization of carbonate from a carbonated silicate melt (Ionov, 1998). The first possibility is in apparent contrast to the experimental

results of Lee & Wyllie (1997, 1998*b*), who showed that Mg-calcite and silicate glass do not behave as immiscible liquids during mantle melting processes. However, Minarik (1998) showed experimentally that immiscible carbonate liquid has convex menisci against the coexisting silicate melt and, because of the higher melt–solid interfacial energy of a carbonate with respect to a silicate melt, the latter selectively wets the grain-edge channels, preventing any contact between carbonate and matrix. Figure 1c shows that the carbonate–silicate glass relationships observed at Gobernador Gregores are very similar to those resulting from Minarik's experiments. We therefore conclude that carbonated silicate melt resulting from melting of Assemblage 2 underwent later immiscibility of the carbonate component, in agreement with evidence from natural samples (Chalot-Prat & Arnold, 1999).

Unmixing occurred before crystallization of the Assemblage 3 minerals, because they are never found inside the carbonate drops or crossing the silicate melt–carbonate contact. U and Sr are highly concentrated in carbonate with respect to the silicate melt, suggesting their preferential entry in the former. As a consequence, the Cpx_3 crystals formed from the silicate melt have U concentration below the detection limit and appreciable Sr negative anomalies (Figs 3a and b and 4).

During flow in a silicate matrix, carbonate melt mobility is severely restricted with respect to that of the silicate melt, thus inducing local enrichment of carbonate and depletion of the silicate melt (Minarik, 1998). As a consequence, the melt unmixing and migration, shown in the Gobernador Gregores xenoliths by the presence of veins originating from the pockets (see previous description), induced variations in bulk-rock composition, in spite of Assemblage 3 production being isochemical.

Assemblage 2: metasomatic agents

Carbonatite metasomatism?

Indicators of metasomatism related to carbonate fluids or melts are, in bulk rock, high CaO/Al_2O_3 and Na_2O/Al_2O_3, a marked tendency towards wehrlite mineralogy, the presence of apatite, enrichment in the jadeite component of clinopyroxene, high La_N/Yb_N, and relative depletions of Ti and Hf with respect to REE and high Ba (Yaxley *et al.*, 1991; Rudnick *et al.*, 1993). Both in bulk rock and mineral phases the iron, aluminium and Ti concentrations should remain virtually unchanged. Applied to the Gobernador Gregores xenoliths, these indicators provide inconclusive evidence. Some of the xenoliths have high CaO/Al_2O_3, but Na_2O/Al_2O_3 is invariably low, indicating only CaO (i.e. carbonate) enrichment. This can be ascribed to the different mobility rate between Assemblage 3 carbonate and silicate melt previously discussed. In some samples, there is a distinct whole-rock enrichment in TiO_2, which in sample GG92 may be as high as 0·33 wt %. The Assemblage 2 pyroxenes are in general richer in Fe and Ti than are those in Assemblage 1. Orthopyroxene in Assemblage 2 is a forming, not a dissolving, phase; the wehrlites do not contain orthopyroxene and may thus be the result of clinopyroxene addition to a dunite, not the result of orthopyroxene dissolution from a lherzolite or harzburgite. Apatite is Cl rich, not F rich as observed in most carbonatites (Hogarth, 1989; Hornig-Kjersgaard, 1998), and sometimes in xenoliths (Hauri *et al.*, 1993; Rudnick *et al.*, 1993). On the other hand, the high Na_2O concentration of Cpx_2 and its trace element characteristics (high La_N/Yb_N; Hf and Ti negative anomalies) are similar to those observed in xenoliths affected by carbonatite metasomatism (Yaxley *et al.*, 1991; Rudnick *et al.*, 1993).

We have estimated the trace element concentration of the metasomatic agent using the Cpx_2 composition and the Cpx_3–glass partition coefficients (Fig. 5c). Although the use of these partition coefficients is questionable in several ways (e.g. low-pressure origin of the glasses, D values referred to solid–melt system applied to a situation where the metasomatic agent may be a fluid), they have at least the advantage of being referred to a chemically closed system, because it has been shown that glass production does not require the introduction of exotic chemical species (except perhaps CO_2). The comparison of the geochemical characteristics of the estimated metasomatic agent with those of crustal carbonatites is inconclusive for two reasons. First, crustal carbonatites are not primary melts (Ionov, 1998), and have, therefore, variable geochemical characteristics depending on their petrogenetic process. Examination of the carbonatite occurrences reported by Nelson *et al.* (1988) reveals that they have highly variable trace element concentrations and variation patterns. They have in common LREE enrichment with respect to HREE and, in most occurrences, Ti and Hf depletion, whereas Th, U, Nb and Ta are extremely variable both in concentration and reciprocal relationships, therefore representing poor indicators of carbonatite metasomatism. Second, the Ti depletion relative to REE of the metasomatic agent here estimated is not as dramatic as in the crustal carbonatites. Furthermore, the CaO/Al_2O_3 variation in whole rock does not correlate with the observed Hf depletion of the metasomatic agent, indicating different controls on the two parameters.

Distinction between carbonatite and silicate melt or fluid metasomatism based on experimental petrology is even more confusing. For example, Wendlandt & Harrison (1979) and Green *et al.* (1992) indicated REE preference for the carbonated melt (although partition coefficients increase for the first researchers, and decrease for the second, from LREE to HREE), whereas, according

to Hamilton *et al.* (1989) and Veksler *et al.* (1998), REE are partitioned into the silicate melt (again with opposite partition coefficient variation from LREE to HREE in the two experiments). Sweeney *et al.* (1995), on the basis of experimental mineral–melt partition coefficients, showed that mantle affected by carbonatite or silicate melt metasomatism would present qualitatively similar patterns but with markedly higher concentrations of Na, Nb, Ta and Sr, and slightly higher Zr in case of carbonatite metasomatism, whereas Ti and HREE are similar in the two cases.

The high Zr/Hf (and Ba/Nb; Green *et al.*, 1992) ratio, held to be a typical effect of carbonatite metasomatism, was found to remain virtually unchanged by Klemme *et al.* (1995). Veksler *et al.* (1998) found that Ta is much more preferentially partitioned into silicate than Nb, resulting in a high Nb/Ta ratio of carbonatite. However, Sweeney *et al.* (1995) did not indicate any Nb–Ta fractionation. This cursory examination of the inconsistencies of published experimental results indicates that element ratios, or element concentrations, cannot provide definite evidence of carbonatite metasomatism.

Silicate melt–fluid metasomatism?

Various workers have shown that metasomatic imprints similar to those brought about by carbonate melts may derive from hydrous silicate melts, either because of the variations in the element partition coefficients on the basis of composition (Vannucci *et al.*, 1998; Wulff-Pedersen *et al.*, 1999), or because of the percolation and reaction mechanism (Zinngrebe & Foley, 1995; Bedini *et al.*, 1997; Zanetti *et al.*, 1999). At Gobernador Gregores, the crystallization rather than dissolution of the orthopyroxene in Assemblage 2 is more indicative of a silicate melt than of a carbonate one.

Hydrous silicate melts occur in several different environments and may have various origins (Schiano *et al.*, 1994). Because of the geodynamic context of Gobernador Gregores, we hypothesize the origin of the metasomatic agent from the subducted slab, which was in eclogite facies at this distance from the trench (400 km). Both the high water and Cl concentrations of the metasomatic agent favour a slab origin, because fluid inclusions and brines in eclogites related to subduction environments are, in addition to H_2O, chloride rich as a response to hydrothermal alteration of the sea floor before subduction (Philippot & Selverstone, 1991; Scambelluri *et al.*, 1997; Philippot *et al.*, 1998). As demonstrated by experimental results (Ayers & Eggler, 1995; Brenan *et al.*, 1995; Bureau & Keppler, 1999) and studies on brines and fluid inclusions in eclogite-facies rocks (Philippot & Selverstone, 1991; Scambelluri *et al.*, 1997), silicate solubility in hydrous fluids increases with temperature, pressure and Cl concentration, so that at high pressure and Cl concentration these fluids are analogues of silicate melts (Ayers & Eggler, 1995). Both fluids and melts are enriched in LREE with respect to HREE, as demonstrated for the latter by the experimental work of Rapp *et al.* (1991), who found that melts of eclogite-facies basaltic charges have La_N/Yb_N ratios as high as 50, comparable with the La_N/Yb_N range (58–70) of the estimated metasomatic agent (Fig. 5c). The main problem concerns HFSE, because it is still a matter of debate whether slab-derived fluids may efficiently transport these elements and whether the HFSE anomalies observed in the xenoliths are slab inherited or acquired during percolation. Regarding the first point, most workers agree that fluids, in addition to REE, can also transport large amounts of HFSE, whose solubility increases at increasing pressure and Cl concentration. Philippot & Selverstone (1991) found brines in eclogites rich in Fe, Ti, P, Ba, Ce, La and Th, and monazite, rutile and sphene as daughter minerals. Brenan *et al.* (1995) indicated Nb, Th, Zr and Hf solubility. As for the origin of the HFSE anomalies, opinions differ widely. For example, the presence of rutile in the experiments of Rapp *et al.* (1991) would induce a large negative Nb anomaly in the slab component, but Ayers & Watson (1993) demonstrated that rutile solubility is pressure dependent. At 3 GPa rutile is $\sim$100 times more soluble than LILE- and REE-enriched monazite, so that fluids may be enriched in Ti, Zr and other HFSE relative to LILE and LREE (Kelemen *et al.*, 1993). However, with the exception of Ryerson & Watson (1987) and Keppler (1996), who suggested that HFSE anomalies may characterize the fluids, most workers claim that variations of element solubility in fluids are not sufficient to induce fractionation either among the HFSE or between HFSE and REE (Ayers & Eggler, 1995; Adam *et al.*, 1997; Ayers *et al.*, 1997). In agreement with these workers, the HFSE concentration and anomalies of the present putative metasomatic agent cannot be explained only by slab-inherited characteristics. This is also the result of studies on the origin of geochemical features in subduction-related magmas (e.g. Kelemen *et al.*, 1990, 1993), inferred to be controlled by percolation and reaction with the mantle wedge. We cannot at present fully document the percolation–reaction process because data are still scarce, but the amphibole composition is sufficient to preliminarily constrain the process and to indicate that percolation-reaction of a subducted slab-derived component is a viable hypothesis for explaining the HFSE anomalies.

Evidence from amphibole

The partition coefficients between amphibole and putative metasomatic agent are shown in Fig. 5d, where they are compared with available literature data. Our data parallel the *D* patterns from the literature, which have an extremely high variation range. Of especial

interest for the present discussion are the Nb, Ta, Hf, Zr and Ti anomalies. Tiepolo *et al.* (2000 and this volume) have shown that partition coefficients of these elements may vary by orders of magnitude, depending on melt and amphibole structure and composition. They found, for example, that $^{Amph/L}D_{Nb}$ and $^{Amph/L}D_{Ta}$ may become as high as 1·63 and 1·0, respectively, in Ti-depleted, dehydrogenated amphiboles (Tiepolo *et al.*, 2000). Similar chemical–crystallographic controls also affect Zr and Hf (Tiepolo *et al.*, 2001) so that in certain circumstances Hf may become compatible.

Pervasive occurrence of Assemblage 2 and the textural characteristics of the xenoliths suggest that the mantle wedge was metasomatized by reactive porous flow. In mantle segments percolated by large fluid volumes, the *mg*-number value of amphibole and of the other phases resulting from reaction is likely to reflect that of the metasomatic agent (Xu *et al.*, 1998) and hence to be relatively low. In segments percolated by small melt volumes, as could be the case in the upper part of the mantle column in the models of Bedini *et al.* (1997) and Vernières *et al.* (1997), the *mg*-number value of amphibole is buffered by that of the peridotite at high *mg*-number values. Therefore, the sample with the lowest *mg*-number amphibole (GG92, *mg*-number 0·84) possibly represents a deeper level of the mantle column, whereas the others (*mg*-number 0·90) represent shallower levels. Partition coefficients for GG92 (Fig 5d) indicate that amphibole crystallization would induce an increase in the LREE/HREE, Nb/Ta, Zr/Hf and Sr/(Pr, Nd) ratios, an increase of Nb and Ta, and a decrease of Ti in the residual liquid. These are the general characteristics observed in the putative metasomatic agent in samples with higher *mg*-number. In these samples $^{Amph/L}D_{Nb} > 1$ is in agreement with that predicted by Tiepolo *et al.* (2000) for amphiboles in equilibrium with SiO_2-saturated, TiO_2-poor melts. Ionov & Hofmann (1995) discussed similar findings and proposed that Nb in certain circumstances (silica-rich hydrous fluids, rather than silicate or carbonate melts) may become compatible in amphibole. The $^{Amph/L}D_{Zr}$ and $^{Amph/L}D_{Hf}$ of GG92 are able to explain the Zr/Hf variation of the other putative liquids referred to lower melt/rock ratios, not their absolute Zr and Hf concentration. Partition coefficients predict that Zr and Hf concentration should increase in the residual liquids, not decrease as observed in the putative melts. To fit the putative melts, both elements should be compatible and Hf more compatible than Zr. This is observed in one of the experimental runs of Tiepolo *et al.* (2001), but not directly documented here. Another possibility is that the low Zr concentrations reflect mixing with the composition of the pre-metasomatic peridotite, which had a dominant effect because of low melt/rock ratio. Further constraints on this model and on the metasomatic process are the subject of work in progress.

CONCLUSION

Mantle xenoliths at Gobernador Gregores (southern Patagonia) provide evidence that a depleted lithospheric mantle suffered a major metasomatic episode, resulting in the recrystallization of all the previous phases and in the addition of amphibole, phlogopite and apatite. Its modal and geochemical signature resembles that believed to be typical of metasomatism brought about by carbonate fluids and melts. However, the lack of unequivocal indicators of carbonatite metasomatism, and deviations from modal and geochemical parameters considered to be typically induced by such a metasomatic agent, suggest that the enrichment episode was caused by other agents. These are inferred to be hydrous fluids or silicate melts, possibly slab derived. The induction of amphibole crystallization, in addition to other modal variations, is an effect of the reactive porous flow of this agent through the mantle wedge. We have estimated the element partitioning between amphibole and the potential metasomatic agent. The results suggest that amphibole crystallization alone is able to induce the observed Ti depletions relative to REE, concomitant with Nb enrichment and a high Zr/Hf ratio. We propose that the xenoliths in which the amphibole has relatively low *mg*-number, marked positive Ti anomaly, modest positive Nb anomaly and $Zr_N/Hf_N \sim 1$ represent the deeper levels of the mantle segment, percolated by large volumes of the metasomatic agent. The xenoliths where amphibole has higher *mg*-number, negative Ti anomaly, marked positive Nb anomaly, and high Zr_N/Hf_N values represent a shallower depth, percolated by smaller volumes of residual metasomatic fluid, whereas the xenoliths that have no sign of metasomatism come from the shallowest levels.

The phases of the metasomatic assemblage, dominantly amphibole, underwent subsequent disequilbrium melting, resulting in the production of a carbonated silicate melt. Mass-balance calculations indicate that the melting process was isochemical, except perhaps for CO_2, which may originate from hypothetical carbonates in the metasomatic assemblage or fluid inclusions in its mineral phases (neither of which has been found), or from degassing during decompression of the transporting basalts. The carbonated silicate melt underwent liquid immiscibility, products of which are now represented by carbonated drops and silicate glass. Olivine, spinel and clinopyroxene, with markedly different compositions from their analogues in the premetasomatic and metasomatic assemblage, crystallized in the silicate melt after unmixing. In addition to pockets principally around relic amphibole, the melting products of the metasomatic assemblage are also observed in veins originating from the pockets and infiltrating along grain edges and fractures. Because of the different flow rate of carbonate with

respect to silicate melt, xenoliths thereby become enriched in CaO. Therefore, the high CaO/Al_2O_3 value often observed in bulk-rock composition and taken as an indicator of carbonatite metasomatism, is in this respect inconclusive, as also suggested by the Na_2O/Al_2O_3 values, which remain invariably low. An obvious consequence of the observed relative chronology between metasomatism and melting is that the carbonated silicate melt cannot be the metasomatic agent, and it is merely the result of decompression melting during uplift of the xenoliths to the surface.

ACKNOWLEDGEMENTS

We thank J.-L. Bodinier, G. Chazot and an anonymous referee for their critical reading, which has improved a first draft of this paper. We are grateful to the director of FOMICRUZ, Ing. A. Traba, for having resolved our travel problems in Patagonia and handling the samples, and to R. Mandelo and J.C. Jaque for assistance during field-work. Mr R. Barrenechea is gratefully acknowledged for the indications on the xenolith localities and for the facilities provided at Gobernador Gregores. Our thanks go to the Municipalidad of Gobernador Gregores for accommodation. This research was financially supported by MURST (COFIN 98), CNR and CNR–CONICET joint programmes. We acknowledge the assistance of Gavin Taylor in linguistic correction of the manuscript.

REFERENCES

Adam, J. & Green, T. H. (1994). The effects of pressure and temperature on the partitioning of Ti, Sr and REE between amphibole, clinopyroxene and basanitic melts. *Chemical Geology* **117**, 219–233.

Adam, J., Green, T. H. & Sie, S. H. (1993). Proton microprobe determined partitioning of Rb, Sr, Ba, Y, Zr, Nb and Ta between experimentally produced amphiboles and silicate melts with variable F content. *Chemical Geology* **109**, 29–49.

Adam, J., Green, T. H., Sie, S. H. & Ryan, C. G. (1997). Trace element partitioning between aqueous fluids, silicate melts and minerals. *European Journal of Mineralogy* **9**, 569–584.

Ayers, J. C. & Eggler, D. H. (1995). Partitioning of elements between silicate melt and H_2O–NaCl fluids at 1·5 and 2·0 GPa pressure: implications for mantle metasomatism. *Geochimica et Cosmochimica Acta* **59**, 4237–4246.

Ayers, J. C. & Watson, E. B. (1993). Rutile solubility and mobility in supercritical fluids. *Contributions to Mineralogy and Petrology* **114**, 321–330.

Ayers, J. C., Dittmer, S. K. & Layne, G. D. (1997). Partitioning of elements between peridotite and H_2O at 2·0–3·0 GPa and 900–1100°C and application to models of subduction zone processes. *Earth and Planetary Science Letters* **150**, 381–398.

Barbieri, M. A., Rivalenti, G., Cingolani, C., Vannucci, R. & Kempton, P. D. (1999). Geochemical and isotope constraints on the composition of the mantle lithosphere in Patagonia (Argentina, Chile). *Proceedings of the II South American Symposium on Isotope Geology*. Cordoba, Argentina: Servicio Geologico Minero Argentino, pp. 163–166.

Bedini, R. M., Bodinier, J.-L., Dautria, J.-M. & Morten, L. (1997). Evolution of LILE-enriched small melt fractions in the lithospheric mantle: a case study from East African Rift. *Earth and Planetary Science Letters* **153**, 67–83.

Bottazzi, P., Tiepolo, M., Vannucci, R., Zanetti, A., Brumm, R., Foley, S. F. & Oberti, R. (1999). Distinct site preferences for heavy and light REE in amphibole and the prediction of $^{Amph/L}D_{REE}$. *Contributions to Mineralogy and Petrology* **137**, 36–45.

Brenan, J. M., Shaw, H. F., Ryerson, F. J. & Phinney, D. L. (1995). Mineral–aqueous fluid partioning of trace elements at 900°C and 2·0 GPa: constraints on the trace element chemistry of mantle and deep crustal fluids. *Geochimica et Cosmochimica Acta* **59**, 3331–3350.

Brey, G. P. & Köhler, T. (1990). Geothermobarometry in four-phase lherzolites. II. New thermobarometers, and practical assessment of existing thermobarometers. *Journal of Petrology* **31**, 1353–1378.

Bureau, H. & Keppler, H. (1999). Complete miscibility between silicate melts and hydrous fluids in upper mantle: experimental evidence and geochemical implications. *Earth and Planetary Science Letters* **165**, 187–196.

Chalot-Prat, F. & Arnold, M. (1999). Immiscibility between calcio-carbonatitic and silicate melts and related wall rock reactions in the upper mantle: a natural case study from Romanian mantle xenoliths. *Lithos* **46**, 627–659.

Chazot, G., Menzies, M. A. & Harte, B. (1996). Determination of partition coefficients between apatite, clinopyroxene, amphibole, and melt in natural spinel lherzolites from Yemen: implications for wet melting of the lithospheric mantle. *Geochimica et Cosmochimica Acta* **60**, 423–437.

Dalpé, C. & Baker, D. R. (1994). Partition coefficients for rare-earth elements between calcic amphibole and Ti-rich basanitic glass at 1·5 GPa, 1100°C. *Mineralogical Magazine* **58A**, 207–208.

Dalton, J. A. & Wood, B. J. (1993*a*). The composition of primary carbonate melts and their evolution through wallrock reaction in the mantle. *Earth and Planetary Science Letters* **119**, 511–525.

Dalton, J. A. & Wood, B. J. (1993*b*). The partitioning of Fe and Mg between olivine and carbonate and the stability of carbonate under mantle conditions. *Contributions to Mineralogy and Petrology* **114**, 501–509.

Dautria, J. M., Dupuy, C., Takherist, D. & Dostal, J. (1992). Carbonate metasomatism in the lithospheric mantle: peridotitic xenoliths from a melilitic district of the Sahara basin. *Contributions to Mineralogy and Petrology* **111**, 37–52.

Gorring, M. L., Kay, S. M., Zeitler, P. K., Ramos, V. A., Rubiolo, D., Fernandez, M. I. & Panza, J. L. (1997). Neogene Patagonian plateau lavas: continental magmas associated with ridge collision at the Chile Triple Junction. *Tectonics* **16**, 1–17.

Green, D. H. & Wallace, M. E. (1988). Mantle metasomatism by ephemeral carbonatite melts. *Nature* **336**, 459–462.

Green, T. H., Adam, J. & Sie, S. H. (1992). Trace element partitioning between silicate minerals and carbonatite at 25 kbar and application to mantle metasomatism. *Mineralogy and Petrology* **46**, 179–184.

Hamilton, D. L., Bedson, P. & Esson, J. (1989). The behaviour of trace element in the evolution of carbonatites. In: Bell, K. (ed.) *Carbonatites—Genesis and Evolution*. Boston, MA: Unwin Hyman, pp. 405–427.

Hauri, E. H., Shimizu, N., Dieu, J. J. & Hart, S. R. (1993). Evidence for hot-spot-related carbonatite metasomatism in the oceanic upper mantle. *Nature* **365**, 221–227.

Hofmann, A. W. (1988). Chemical differentiation of the Earth: the relationship between mantle, continental crust, and oceanic crust. *Earth and Planetary Science Letters* **90**, 297–314.

Hogarth, D. D. (1989). Pyrochlore, apatite and amphibole: distinctive minerals in carbonatite. In: Bell, K. (ed.) *Carbonatites—Genesis and Evolution*. Boston, MA: Unwin Hyman, pp. 105–148.

Hornig-Kjarsgaard, I. (1998). Rare earth elements in sovitic carbonatites and their mineral phases. *Journal of Petrology* **39**, 2105–2122.

Ionov, D. A. (1998). Trace element composition of mantle-derived carbonates and coexisting phases in peridotite xenoliths from alkali basalts. *Journal of Petrology* **39**, 1931–1941.

Ionov, D. A. & Hofmann, A. W. (1995). Nb–Ta-rich amphiboles and micas: implications for subduction-related metasomatic trace element fractionation. *Earth and Planetary Science Letters* **131**, 341–356.

Ionov, D. A., Dupuy, C., O'Reilly, S. Y., Kopylova, M. G. & Genshaft, Y. S. (1993). Carbonated peridotite xenoliths from Spitsbergen: implications for trace element signature of mantle carbonate metasomatism. *Earth and Planetary Science Letters* **119**, 283–297.

Ionov, D. A., Hofmann, A. W. & Shimizu, N. (1994). Metasomatism-induced melting in mantle xenoliths from Mongolia. *Journal of Petrology* **35**, 753–785.

Ionov, D. A., O'Reilly, S. Y., Genshaft, Y. S. & Kopylova, M. G. (1996). Carbonate-bearing mantle peridotite xenoliths from Spitsbergen: phase relationships, mineral composition and trace-element residence. *Contributions to Mineralogy and Petrology* **125**, 375–392.

Jeffries, T. E., Jackson, S. E. & Longerich, H. P. (1998). Application of a frequency quintupled Nd:YAG source (l = 213 nm) for laser ablation inductively coupled plasma mass spectrometric analysis of minerals. *Journal of Analytical Atomic Spectroscopy* **13**, 935–940.

Johnson, K. T. M., Davis, A. M. & Bryndzia, L. T. (1996). Contrasting styles of hydrous metasomatism in the upper mantle: an ion microprobe investigation. *Geochimica et Cosmochimica Acta* **60**, 1367–1385.

Kelemen, P. B., Johnson, K. T. M., Kinzler, R. J. & Irving, A. J. (1990). High-field-strength element depletions in arc basalts due to mantle–magma interactions. *Nature* **345**, 521–524.

Kelemen, P. B., Shimizu, N. & Dunn, T. (1993). Relative depletion of niobium in some arc magmas and the continental crust: partitioning of K, Nb, La and Ce during melt/rock reaction in the upper mantle. *Earth and Planetary Science Letters* **120**, 111–134.

Keppler, H. (1996). Constraints from partitioning experiments on the composition of subduction-zone fluids. *Nature* **380**, 237–240.

Klemme, S., van der Laan, S. R., Foley, S. F. & Gunther, D. (1995). Experimentally determined trace and minor element partitioning between clinopyroxene and carbonatite melt under upper mantle conditions. *Earth and Planetary Science Letters* **133**, 439–448.

Kogarko, L. N., Henderson, C. M. B & Pacheco, H. (1995). Primary Ca-rich carbonatite magma and carbonate–silicate–sulphide liquid immiscibility in the upper mantle. *Contributions to Mineralogy and Petrology* **121**, 267–274.

Köhler, T. P. & Brey, G. P. (1990). Calcium exchange between olivine and clinopyroxene calibrated as a geothermobarometer for natural peridotites from 2 to 60 kbar with applications. *Geochimica et Cosmochimica Acta* **54**, 2375–2388.

Lee, W.-J. & Wyllie, J. P. (1997). Liquid immiscibility between nephelinite and carbonatite from 1·0 to 2·5 GPa compared with mantle melt compositions. *Contributions to Mineralogy and Petrology* **127**, 1–16.

Lee, W.-J. & Wyllie, J. P. (1998*a*). Petrogenesis of carbonatite magmas from mantle to crust, constrained by the system $CaO-(MgO + FeO^*)-(Na_2O + K_2O)-(SiO_2 + Al_2O_3 + TiO_2)-CO_2$. *Journal of Petrology* **39**, 495–517.

Lee, W.-J. & Wyllie, J. P. (1998*b*). Processes of crustal carbonatite formation by liquid immiscibility and differentiation, elucidated by model systems. *Journal of Petrology* **39**, 2005–2013.

Maury, R. C., Defant, M. J. & Joron, J.-L. (1992). Metasomatism of the sub-arc mantle inferred from trace elements in Philippine xenoliths. *Nature* **360**, 661–663.

Mazzucchelli, M., Rivalenti, G., Vannucci, R., Bottazzi, P., Ottolini, L., Hofmann, A. W., Sinigoi, S. & Demarchi, G. (1992). The trace element distribution between clinopyroxene and garnet in gabbroic rocks of the deep crust: an ion microprobe study. *Geochimica et Cosmochimica Acta* **56**, 2372–2385.

McDonough, W. F. (1990). Constraints on the composition of the continental mantle. *Earth and Planetary Science Letters* **101**, 1–18.

McKenzie, D. & O'Nions, R. K. (1991). Partial melt distributions from inversion of rare earth element concentrations. *Journal of Petrology* **32**, 1021–1091.

Minarik, W. G. (1998). Complications to carbonate melt mobility due to the presence of an immiscible silicate melt. *Journal of Petrology* **39**, 1965–1973.

Nelson, D. R., Chivas, A. R., Chappell, B. W. & McCulloch, M. T. (1988). Geochemical and isotopic systematics in carbonatites and implications for the evolution of ocean-island sources. *Geochimica et Cosmochimica Acta* **52**, 1–17.

Norman, M. D. (1998). Melting and metasomatism in the continental lithosphere: laser ablation ICPMS analysis of minerals in spinel lherzolites from eastern Australia. *Contributions to Mineralogy and Petrology* **130**, 240–255.

O'Reilly, S. Y. & Griffin, W. L. (1988). Mantle metasomatism beneath western Victoria, Australia: I. Metasomatic processes in Cr-diopside lherzolites. *Geochimica et Cosmochimica Acta* **52**, 433–447.

O'Reilly, S. Y., Griffin, W. L. & Ryan, C. G. (1991). Residence of trace elements in metasomatized spinel lherzolite xenoliths: a proton-microprobe study. *Contributions to Mineralogy and Petrology* **109**, 98–113.

Philippot, P. & Selverstone, J. (1991). Trace-element-rich brines in eclogitic veins: implications for fluid composition and transport during subduction. *Contributions to Mineralogy and Petrology* **106**, 417–430.

Philippot, R., Agrinier, P. & Scambelluri, M. (1998). Chlorine cycling during subduction of altered oceanic crust. *Earth and Planetary Science Letters* **161**, 33–44.

Pyle, J. M. & Haggerty, S. E. (1994). Silicate–carbonate liquid immiscibility in upper mantle eclogites: implications for natrosilicic and carbonatitic conjugate melts. *Geochimica et Cosmochimica Acta* **58**, 2997–3011.

Rapp, R. P., Watson, E. B. & Miller, C. F. (1991). Partial melting of amphibolite/eclogite and the origin of Archean trondhjemites and tonalites. *Precambrian Research* **51**, 1–25.

Rivalenti, G., Mazzucchelli, M., Girardi, V. A. V., Vannucci, R., Barbieri, M. A., Zanetti, A. & Goldstein, S. L. (2000). Composition and processes of the mantle lithosphere in Northeastern Brazil and Fernando de Noronha: evidence from mantle xenoliths. *Contributions to Mineralogy and Petrology* **138**, 308–325.

Rudnick, R. L., McDonough, W. F. & Chappell, B. C. (1993). Carbonatite metasomatism in the northern Tanzanian mantle. *Earth and Planetary Science Letters* **114**, 463–475.

Ryerson, F. J. & Watson, E. B. (1987). Rutile saturation in magmas: implications for Ti–Nb–Ta depletion in island-arc basalts. *Earth and Planetary Science Letters* **86**, 225–239.

Scambelluri, M., Piccardo, G. B., Philippot, P., Robbiano, A. & Negretti, L. (1997). High salinity fluid inclusions formed from recycled seawater in deeply subducted alpine serpentinite. *Earth and Planetary Science Letters* **148**, 485–499.

Schiano, P., Clocchiatti, R., Shimizu, N., Weiss, D. & Mattielli, N. (1994). Cogenetic silica-rich and carbonate-rich melts trapped in mantle minerals in Kerguelen ultramafic xenoliths: implications for metasomatism in the oceanic upper mantle. *Earth and Planetary Science Letters* **123**, 167–178.

Stern, C. R., Frey, F. A., Futa, K., Zartman, R. E. & Kyser, T. K. (1990). Trace-element and Sr, Nd, Pb, and O isotopic compositions of Pliocene and Quaternary alkali basalts of the Patagonian Plateau lavas of southernmost South America. *Contributions to Mineralogy and Petrology* **104**, 294–308.

Sweeney, R. J., Green, D. H. & Sie, S. H. (1992). Trace and minor element partitioning between garnet and amphibole and carbonatitic melt. *Earth and Planetary Science Letters* **113**, 1–14.

Sweeney, R. J., Prozesky, V. & Przybylowicz, W. (1995). Selected trace and minor element partitioning between peridotite minerals and carbonatite melts at 18–46 kbar pressure. *Geochimica et Cosmochimica Acta* **59**, 3671–3683.

Szabo, Cs., Vaselli, O., Vannucci, R., Bottazzi, P., Ottolini, L., Coradossi, N. & Kubovics, I. (1995). Ultramafic xenoliths from the Little Hungarian Plain (Western Hungary): a petrologic and geochemical study. *Acta Vulcanologica* **7**, 249–263.

Szabo, Cs., Bodnar, R. J. & Sobolev, A. V. (1996). Metasomatism associated with subduction-related, volatile-rich silicate melt in the upper mantle beneath the Nógrád–Gömör Volcanic Field, Northern Hungary/Southern Slovakia: evidence from silicate melt inclusions. *European Journal of Mineralogy* **8**, 881–899.

Tiepolo, M. (1999). Determinazione sperimentale dei coefficienti di distribuzione solido–liquido in anfiboli di mantello: ruolo del controllo cristallochimico. Ph.D. thesis, Università degli Studi di Pavia, 314 pp.

Tiepolo, M., Vannucci, R., Oberti, R., Foley, S., Bottazzi, P. & Zanetti, A. (2000). Nb and Ta incorporation and fractionation in Ti-rich pargasite and kaersutite: crystal-chemical constraints and implications for natural systems. *Earth and Planetary Science Letters* **176**, 185–201.

Tiepolo, M., Bottazzi, P., Foley, S., Oberti, R., Vannucci, R., & Zanetti, A. (2001). Fractionation of Nb and Ta from Zr and Hf at mantle depths: the role of titanian pargasite and kaersutite. *Journal of Petrology* **42**, 221–232.

Vannucci, R., Bottazzi, P., Wulff-Pedersen, E. & Neumann, E.-R. (1998). Partitioning of REE, Y, Sr, Zr and Ti between clinopyroxene and silicate melts in the mantle under La Palma (Canary Islands): implications for the nature of the metasomatic agents. *Earth and Planetary Science Letters* **158**, 39–51.

Veksler, V., Petibon, C., Jenner, J. A., Dorfman, A. M. & Dingwell, D. B. (1998). Trace element partitioning in immiscible silicate–carbonate systems: an initial experimental study using a centrifuge autoclave. *Journal of Petrology* **39**, 2095–2104.

Vernières, J., Godard, M. & Bodinier, J.-L. (1997). A plate model for the simulation of trace element fractionation during partial melting and magma transport in the Earth's upper mantle. *Journal of Geophysical Research* **102**, 24771–24784.

Vidal, Ph., Dupuy, C., Maury, R. & Richard, M. (1989). Mantle metasomatism above subduction zones: trace-element and radiogenic isotope characteristics of peridotite xenoliths from Batan Island (Philippines). *Geology* **17**, 1115–1118.

Wendlandt, R. F. & Harrison, W. J. (1979). Rare earth partitioning between immiscible carbonate and silicate liquids and CO_2 vapor: results and implications for the formation of light rare earth-enriched rocks. *Contributions to Mineralogy and Petrology* **69**, 409–419.

Witt-Eickschen, G. & Harte, B. (1994). Distribution of trace elements between amphibole and clinopyroxene from mantle peridotites of the Eifel (Western Germany). *Chemical Geology* **117**, 235–250.

Wulff-Pedersen, E., Neumann, E.-R., Vannucci, R., Bottazzi, P. & Ottolini, L. (1999). Silicic melts produced by reaction between peridotite and infiltrating basaltic melts: ion probe data on glasses and minerals in veined xenoliths from La Palma, Canary Islands. *Contributions to Mineralogy and Petrology* **137**, 59–82.

Xu, Y.-G., Menzies, M. A., Bodinier, J.-L., Bedini, R. M., Vroon, P. & Mercier, J.-C. C. (1998). Melt percolation and reaction atop a plume: evidence from the poikiloblastic peridotite xenoliths from Borée (Massif Central, France). *Contributions to Mineralogy and Petrology* **132**, 65–84.

Yaxley, G. M. & Kamenetsky, V. (1999). *In situ* origin for glass in mantle xenoliths from southeastern Australia: insights from trace element compositions of glasses and metasomatic phases. *Earth and Planetary Science Letters* **172**, 97–109.

Yaxley, G. M., Green, D. H. & Kamenetsky, V. (1998). Carbonatite metasomatism in the southeastern Australian lithosphere. *Journal of Petrology* **39**, 1917–1930.

Yaxley, G. M., Crawford, A. J. & Green, D. H. (1991). Evidence for carbonatite metasomatism in spinel peridotite xenoliths from western Victoria, Australia. *Earth and Planetary Science Letters* **107**, 305–317.

Zanetti, A., Mazzucchelli, M., Rivalenti, G. & Vannucci, R. (1999). The Finero phlogopite-peridotite massif: an example of subduction-related metasomatism. *Contributions to Mineralogy and Petrology* **134**, 107–122.

Zinngrebe, E. & Foley, S. F. (1995). Metasomatism in mantle xenoliths from Gees, West Eifel, Germany: evidence for the genesis of calc-alkaline glasses and metasomatic Ca-enrichment. *Contributions to Mineralogy and Petrology* **122**, 79–96.